

PHYSICS OF THE NEUPERT EFFECT: ESTIMATES OF THE EFFECTS OF SOURCE ENERGY, MASS TRANSPORT, AND GEOMETRY USING *RHESSI* AND *GOES* DATA

ASTRID M. VERONIG,^{1,2} JOHN C. BROWN,³ BRIAN R. DENNIS,² RICHARD A. SCHWARTZ,^{2,4}
 LINHUI SUI,^{2,5} AND A. KIMBERLEY TOLBERT^{2,4}

Received 2004 February 11; accepted 2004 November 8

ABSTRACT

The “empirical Neupert effect” (ENE) is the observed temporal correlation of the hard X-ray (HXR) flux $F_{\text{HXR}}(t)$ with the time derivative of the soft X-ray (SXR) flux $\dot{F}_{\text{SXR}}(t)$ in many flares. This is widely taken to mean that the energetic electrons responsible for $F_{\text{HXR}}(t)$ by thick-target collisional bremsstrahlung are the main source of heating and mass supply (via chromospheric evaporation) of the SXR-emitting hot coronal plasma. If this interpretation were correct, one would expect better correlation between the beam power supply $P_{\text{beam}}(t)$, inferred from the HXR spectrum, and the actual power $P_{\text{in}}(t)$ required to explain the SXR flux and spectrum, allowing for variations in both emission measure (EM) and temperature T , for radiative and conductive cooling losses, and for complexities of geometry like multiple loops. We call this the “theoretical Neupert effect” (TNE). To test if it is true that $P_{\text{beam}}(t)$ and $P_{\text{in}}(t)$ inferred from data are better correlated than $F_{\text{HXR}}(t)$ and $\dot{F}_{\text{SXR}}(t)$, we use an approximate approach for a simple single-loop geometry and rough estimates of the particle and energy transport and apply the model to *RHESSI* and *GOES* data on four flares. We find that if the beam low cutoff energy E_1 is taken as constant, the correlation of $P_{\text{beam}}(t)$, $P_{\text{in}}(t)$ is no better than that of $F_{\text{HXR}}(t)$, $\dot{F}_{\text{SXR}}(t)$. While our modeling contains many approximations to cooling and other physics, ignored entirely from ENE data considerations, there seems to be no reason why their order-of-magnitude inclusion should make the TNE worse rather than better, although this should be checked by more accurate simulations. These results suggest that one or more of the following must be true: (1) fast electrons are *not* the main source of SXR plasma supply and heating, (2) the beam low cutoff energy varies with time, or (3) the TNE is strongly affected by source geometry. These options are discussed in relation to possible future directions for TNE research.

Subject headings: Sun: flares — Sun: X-rays, gamma rays

Online material: color figures

1. INTRODUCTION

Neupert (1968) was the first to note that in the impulsive flare phase the soft X-ray (SXR) flux $F_{\text{SXR}}(t)$ shows a tendency to resemble the cumulative time integral of the microwave flux. Later, such correlations were also observed for the SXR flux and the cumulative time integral of the hard X-ray (HXR) flux $F_{\text{HXR}}(t)$, i.e.,

$$F_{\text{SXR}}(t) \propto \int_{t_0}^t F_{\text{HXR}}(t') dt', \quad (1)$$

or, likewise,

$$\frac{d}{dt} F_{\text{SXR}}(t) \propto F_{\text{HXR}}(t). \quad (2)$$

It was proposed that this empirical relationship, called the “Neupert effect” (NE) by Hudson (1991), provides evidence for a causal relationship between the nonthermal and thermal

flare emissions—in particular, that the instantaneous SXR emission is related to the accumulated energy deposited by non-thermal electrons up to that time (Neupert 1968; Brown 1971; Hudson 1972). Thus, the HXR emission is interpreted as a prompt diagnostic of the instantaneous electron beam power being injected into the flaring atmosphere, whereas the SXR emission is related to the cumulative energy stored in the thermal plasma that was heated by the same accelerated electrons.

Observational statistics show that the NE may be violated in up to half of the events in terms of relative timing between SXR and HXR emissions (Dennis & Zarro 1993; McTiernan et al. 1999; Veronig et al. 2002b). Although other interpretations are possible (as discussed later), deviations from the NE are often interpreted as evidence that the hot SXR-emitting plasma is not heated exclusively by the accelerated electrons causing the observed HXR emission (e.g., Dennis & Zarro 1993). (This is certainly often true outside the HXR impulsive phase, such as when strong preheating is seen in SXR [e.g., Webb 1985; Veronig et al. 2002c].) In addition, from the simple relationship expressed in equation (1), it is expected that the SXR peak flux distribution function, $N(F_{\text{SXR}}) \propto (F_{\text{SXR}})^{-\alpha}$, should have the same power-law index α as the HXR fluence distribution, but this is not the case (see Lee et al. 1995, Veronig et al. 2002a, and references therein). Recently, Veronig et al. (2002b) reconfirmed this inconsistency by directly comparing SXR peak fluxes with corresponding HXR fluences for a large sample of events. For individual events, Feldman (1990) has claimed that the lack of a clear NE relationship in the SXR-HXR data refutes the whole idea of heating of the SXR plasma by particle beams.

¹ Institute for Geophysics, Astrophysics and Meteorology, University of Graz, A-8010 Graz, Austria.

² Laboratory for Astronomy and Solar Physics, NASA Goddard Space Flight Center, Code 682, Greenbelt, MD 20771.

³ Astronomy and Astrophysics Group, Department of Physics and Astronomy, University of Glasgow, Glasgow G12 8QQ, UK.

⁴ Science Systems and Applications, Inc. (SSAI), Lanham, MD 20771.

⁵ Department of Physics, Catholic University of America, 620 Michigan Avenue, Washington, DC 20064.

However, it has to be noted that these empirical observational studies of the NE generally rely solely on comparison of SXR and HXR fluxes, which we henceforth call the “empirical Neupert effect” (ENE). This is obviously not a complete approach in terms of physics, since (1) the SXR and HXR fluxes in specified wavelength bands are not simply proportional to the plasma thermal energy content and beam power, respectively; (2) some of the beam power goes into other forms (conduction, radiation loss, chromospheric heating); (3) the HXR flux and beam power vary in different ways with beam spectral index and low cutoff energy; and (4) modeling in terms of single monolithic loops may be too simplistic as compared to summing contributions from many independent or sequential events on size scales below the resolution of current HXR instruments. If the “theoretical Neupert effect” (TNE) is that changes in the SXR plasma thermal energy content are driven by beam energy input, then one does *not* expect a precise relationship of the form $F_{\text{HXR}}(t) \propto \dot{F}_{\text{SXR}}(t)$. Rather, one expects a relationship more like the following: beam power into corona = rate of change of hot plasma thermal energy content + cooling losses.

To date, numerous authors have run hydrodynamic simulations using one-dimensional monolithic loop models, although some progress is being made on quasi-two-dimensional modeling (e.g., Hori et al. 1997, 1998; Reeves & Warren 2002). In particular, Li et al. (1993) have performed such one-dimensional hydrodynamic simulations of the TNE by calculating SXR and HXR time profiles for both thermal and thick-target electron-heated models. Whereas in a thermal model, in which the SXR source is heated by an unspecified nonparticle process and the HXRs are thermal, no correspondence was found between the HXR time profile and the SXR derivative. In the nonthermal beam model the calculated light curves generally revealed good similarity to the alleged Neupert light-curve effect. However, for gradual events the coherence breaks down, with the SXR emission decreasing once the saturation of the evaporation process (and of the emission measure) cannot overcome the rapid cooling of the hot plasma by thermal conduction (Li et al. 1993). These calculations are based on a simple ad hoc parametric model for the electron beam input time profile [and hence for $F_{\text{HXR}}(t)$] and predict theoretical $F_{\text{SXR}}(t)$ via $\text{EM}(t)$, $T(t)$. These show that in such a model the Neupert X-ray flux effect for simulated data is realized, except in gradual events. Here we address whether this is true for real data on the HXR beam input and SXR thermal plasma. (The fact that in a simulation beam heating alone would produce an NE does not prove that an observed NE is produced by beam heating—only that it is consistent with such a model, e.g., the HXR beam heating flux might correlate well in time with a much larger heating process.)

On the basis of very simple models of the source energy budget and one-dimensional geometry, we compare for several real flares the total rate of change of the SXR plasma energy content with the injected electron beam power, using *RHESSI* HXR and SXR observations in combination with *GOES* SXR data. A range for the total net hot plasma power input is estimated from the SXR data, taking into account its variable mass; rough estimates of its thermal, kinetic, and gravitational energies; and losses by conduction and radiation. The actual electron beam power injected into the hot plasma is derived from HXR spectra assuming a collisional thick-target model (Brown 1971). Our first aim is to see whether including the estimates of effects (1)–(3) in the modeling data indeed gives a TNE correlation that is any better than that of the ENE and to discuss the relationship of the findings to consideration (4).

2. EMPIRICAL THEORETICAL NEUPERT EFFECT MODEL

In this section we develop a simple one-dimensional energy transport model of the TNE, replacing a full hydrodynamic treatment by using upper and lower bound estimates of hot plasma energy content for a range of ratios of, e.g., kinetic and gravitational energy content to enthalpy (for an analytic approach, see also Fisher & Hawley 1990). In doing so we adopt a single, monolithic, one-dimensional loop model. This is in line with most past modeling efforts and with the simple SXR-HXR loops with two HXR footpoints that are commonly seen, including those in our events. We recognize that there is evidence from the *Transition Region and Coronal Explorer (TRACE)* (e.g., Schrijver et al. 1999; Warren 2000) for the presence of moving bright footpoints and more complex postflare EUV loop structure, although where their connection with the impulsive phase action lies is not established (as discussed in § 6.8).

The total SXR plasma ($\geq 10^7$ K) energy content at time t , $U_S(t)$, is made up of the thermal energy $U_{\text{th}}(t)$, the kinetic energy $U_k(t)$, and the gravitational energy $U_g(t)$:

$$U_S(t) = U_{\text{th}}(t) + U_k(t) + U_g(t). \quad (3)$$

For a fully ionized plasma, the thermal energy is given by

$$U_{\text{th}}(t) = 3n(t)kT(t)V, \quad (4)$$

where n is the (mean) density, T is the (mean) temperature, and V is the volume of the hot plasma. From *RHESSI* observations we infer an estimate of the hot loop volume V from measures of the area A and separation d of the footpoints seen in HXRs. Assuming a simple, monolithic, one-dimensional, cylindrical single-loop geometry, the volume is given by $V = Al$, with the loop length $l = \pi d/2$. For such geometry the density n can be inferred from the observed emission measure (EM) and the volume V of the source (assumed constant over the flare duration),

$$n(t) = \left[\frac{\text{EM}(t)}{V} \right]^{1/2}, \quad (5)$$

assuming a filling factor of unity (see the discussion of filling factor effects in § 6.3). Thus, the thermal energy can be expressed in terms of the observables as

$$U_{\text{th}}(t) = 3kT(t)[\text{EM}(t)V]^{1/2}. \quad (6)$$

In a closed tube of increasing hot plasma mass, work is done against pressure as well as in increasing T , so the total internal-thermal energy can actually be higher than this because of the compressional increase in energy density as density rises. This could raise U_{th} by up to the specific heat ratio $c_p/c_V \approx 5/3$ for constant pressure versus constant volume heating.

To properly infer the gravitational energy U_g and the kinetic energy U_k , plasma height and speed information are needed; this is observationally difficult and theoretically requires use of a hydrodynamic code. However, U_g (uplift) and U_k (acceleration) are—unless driven magnetically—driven by the pressure gradient, i.e., by U_{th} . Here we simply put bounds on U_S by evaluating the extreme cases. In particular, in the extreme case of equipartition over all forms, we expect that an amount as large as

$$U_k(t) \sim U_g(t) \approx U_{\text{th}}(t) \quad (7)$$

could be added to the estimate of the total internal energy estimated by equation (6). Consequently, we replace a full hydrodynamic treatment by putting upper and lower bounds on our estimate of observed SXR plasma energy content, viz.,

$$3kT(t)[EM(t)V]^{1/2} \lesssim U_S(t) \lesssim 10kT(t)[EM(t)V]^{1/2}. \quad (8)$$

In practice, our loop length is much less than the hydrostatic scale height at temperature T , i.e., $m_p g l \ll kT$, so $U_g \ll U_{th}$; however, we include U_g for general loop lengths and to be generous in our bounds on U_S .

Heating, e.g., by an electron beam with power P_{in} , has to not only provide the observed increase of the SXR plasma energy content, $\dot{U}_S(t)$, but it also has to offset losses by radiation, $L_{rad}(t)$, and by conduction, $L_{cond}(t)$; i.e.,

$$P_{in}(t) = \dot{U}_S(t) + L_{rad}(t) + L_{cond}(t) \text{ ergs s}^{-1}. \quad (9)$$

The radiative losses are given by

$$L_{rad}(t) = EM(t)f_{rad}[T(t)] \text{ ergs s}^{-1}. \quad (10)$$

The radiative loss function, $f_{rad}(T)$, for solar abundances and ionization equilibrium is given by, e.g., Cox & Tucker (1969) and can be approximated in the range of $10^5 \text{ K} \lesssim T \lesssim 30 \text{ MK}$ by

$$f_{rad}(T) \approx 6 \times 10^{-22} (T/10^5)^{-1/2}. \quad (11)$$

At the loop-top temperatures we are considering, it is expected that conduction is a loss term in the energy equation—a fact born out by full hydrodynamic simulations such as Li et al. (1993). This heat “loss” from the hot plasma, apart from that lost by radiation, is of course delivered into the cooler chromosphere, adding to the beam-driven evaporation of additional loop mass and to the loop SXR EM once the material there is heated to SXR temperatures. Thus, conduction acts indirectly as a gain term in the continuity equation. Since our loop mass and EM are based on observations, that conductively driven inflow of mass is included in our treatment. Properly dealing with conduction and evaporation without a full code is difficult, as they depend on gradients and timescales. Energy lost from the hot plasma into the chromosphere by conduction and the beam tail result in heating up to the radiatively unstable evaporation temperature and then to SXR temperatures. However, a large fraction of the power so deposited is lost to the very strong radiative cooling near the cooling function peak. Without a full code the fraction returned to the hot plasma is hard to assess. For testing, we have run our calculations with no conduction. We find that with the best value of the low cutoff energy (a few keV higher than in our model), the cross-correlation of the power time profiles is even worse. On the other hand, if we assumed that all energy entering the chromosphere were lost to radiation, there would be no evaporative increase in EM, contrary to observations. This suggests that our approximation is closer to the truth than either of these extremes.

In the hot plasma energy equation, the conductive losses are given by

$$L_{cond}(t) = AF_{cond}[T(t)] \text{ ergs s}^{-1}, \quad (12)$$

where the conductive flux $F_{cond}(T)$ out of both ends of the loop can be roughly estimated from the observed parameters as

$$F_{cond}(T) = \kappa_0 T^{5/2} \nabla T \approx \frac{4}{7} \kappa_0 T^{7/2}, \quad (13)$$

with $\kappa_0 = 10^{-6} \text{ ergs cm}^{-1} \text{ s}^{-1} \text{ K}^{-7/2}$, the classical Spitzer coefficient for thermal conduction. Here l is the temperature scale length at the peak temperature T (and decreases at low temperatures). The relationship of this rough approximation to the full conduction equation and hydrodynamic codes is discussed in the literature (e.g., Hawley & Fisher 1994).

Equations (8), (9), (10), and (12), together with the inferred flare size parameters, let us estimate the total P_{in} needed at any time t to yield a measured $\dot{U}_S(t)$ from observed variations of $EM(t)$ and $T(t)$. For a single loop the TNE is then the equating of the measured thermal $P_{in}(t)$ with the electron beam power input into the hot part of the loop (i.e., above the transition zone), $P_{beam}(t)$.

The other fraction of the beam reaches the chromosphere and causes heating there. As a consequence, when heated to above $\sim 60,000 \text{ K}$, chromospheric matter becomes radiatively unstable and expands upward into the coronal loop (“chromospheric evaporation”; Sweet 1969; Brown 1973; Antiochos & Sturrock 1978). Such matter constitutes the “transition region” between the stable cool and hot atmospheric components, although it is now recognized that, instead of being a simple stratified structure, it will be fragmented by unstable convection into what is observed as “moss” (e.g., Berger et al. 1999).

We are considering here the energy budget of the hot SXR-emitting plasma mass $U_{th} \simeq 3NkT \simeq 3nVkT$. The energy content of this can increase (or decrease) by two processes: (1) the increase (or decrease) ΔT of its temperature and (2) the addition (or removal) ΔN of particles in it. The release of energy in the SXR plasma by beam heating raises T and U_{th} directly ($\Delta U_{th} = 3Nk\Delta T$). This involves the fraction ϕ of the total beam power P_1 , according to the coronal column density. The remaining fraction $(1 - \phi)$ of the beam power goes into heating the chromosphere, an upper part of which evaporates by radiative instability, increasing N (and hence increasing ϕ). Having entered the radiative instability regime ($T \gtrsim 10^5 \text{ K}$) by the (increased) beam deposition increases U_{th} ($\Delta U_{th} = 3\Delta NkT$). Thus, the beam power deposited in the chromosphere adds to U_{th} via ΔN . In events in which conductive evaporation is important, some of the energy lost from the hot loop by conduction is returned to the upper loop as conductively evaporated material, again heated to high temperatures by the beam power deposited there. In our analysis N is found from data, not theory, and thus includes both beam and conductively driven parts. In short, ΔU arises from ΔT and ΔN , ΔT being driven by ϕP_1 (less cooling) and ΔN being driven by $(1 - \phi)P_1$ + conductive effects. Of course, not all of the beam and conductive power entering the chromosphere is returned to the corona, since the material radiates during evaporation.

HXR spectra measured with *RHESSI* are used to derive the thick-target electron beam injection rate $F_1(t)$ (electrons s^{-1}) at energies $E > E_1$ for low cutoff energy E_1 with electron spectral index $\delta(t)$ (based on Brown 1971). Here we only want the part of the beam power injected, $P_1(t)$, given as

$$P_1(t) = \frac{[\delta(t) - 1]}{[\delta(t) - 2]} F_1(t) E_1 \text{ ergs s}^{-1}, \quad (14)$$

that goes into the hot part of the loop, namely,

$$P_{\text{beam}}(t) = P_1(t)\phi(t). \quad (15)$$

The fraction ϕ depends on the loop leg column density N above the transition zone, given by

$$N(t) = n(t) \frac{l}{2} = \left[\frac{\text{EM}(t)}{V} \right]^{1/2} \frac{l}{2} \text{ cm}^{-2}. \quad (16)$$

Since EM varies with time as a result of the evaporation of material into the loop, so does the column density N and $\phi(N)$. On the basis of N derived from SXR data, we can estimate the energy $E_{\text{loop}} > E_1$ of electrons stopped above the transition zone in the hot part of the loop. This is (Brown 1973)

$$E_{\text{loop}}(t) = [3KN(t)]^{1/2}, \quad (17)$$

where $K = 2\pi e^4 \Lambda$ is the collisional stopping parameter, where e is the electron charge and $\Lambda \approx 20$ is the Coulomb logarithm. The fraction ϕ of the beam power going into the hot part of the loop is given by (see Brown 1973)

$$\phi(t) = 1 - \frac{[\delta(t) - 2]}{2} B \left[\frac{\delta(t)}{2} - \frac{1}{2}, \frac{3}{2} \right] \left[\frac{E_{\text{loop}}(t)}{E_1} \right]^{-\delta(t)+2}, \quad (18)$$

where $B(a, b)$ is the complete beta function. The low cutoff energy E_1 is very uncertain, and we handle it as a free parameter. In particular, we investigate whether it is possible to find a constant E_1 (in principle, E_1 may change in time) for which $P_{\text{in}}(t)$ and $P_{\text{beam}}(t)$ show reasonable agreement in terms of the shape of the time series as well as the total energies over the flare duration, considering the crudeness of our energy equation and the substitution of our band of U_S values in place of a hydrodynamic code. In addition, using *RHESSI*'s high spectral resolution, we can evaluate the X-ray spectra in order to see if they are consistent with E_1 derived in this way.

3. THE *RHESSI* INSTRUMENT

The Reuven Ramaty High-Energy Solar Spectroscopic Imager (*RHESSI*), launched on 2002 February 5, is a NASA Small Explorer (SMEX) mission designed to study high-energy emission from solar flares over a broad range, 3 keV to 17 MeV, i.e., from thermal X-rays to γ -rays (Lin et al. 2002). The primary scientific objective of the *RHESSI* mission is to study particle acceleration, energy release, and particle and energy transport in solar flares. The new approach of *RHESSI* is to combine for the first time high-resolution imaging in SXRs ($\geq 10^7$ K), HXR, and γ -rays with high-resolution spectroscopy.

The energy range covered by *RHESSI* (3 keV–17 MeV) requires the use of indirect imaging techniques. *RHESSI*'s imaging capability is based on nine pairs of fine tungsten-molybdenum grids that modulate the incident solar X-ray and γ -ray flux as the spacecraft rotates at ~ 15 revolutions per minute. Ground-based software (Schwartz et al. 2002) is used to reconstruct images of the source from the time-modulated light curves (for details on the *RHESSI* imaging concept, see Hurford et al. 2002). The FWHM spatial resolution is as high as $2''/3$ with a full-Sun field of view.

The high-resolution spectroscopy is achieved by means of nine cryogenically cooled germanium detectors, one behind each rotating modulation collimator (the characteristics of the *RHESSI* spectrometer can be found in Smith et al. 2002). The spectral

resolution is ~ 1 keV FWHM in the SXR-HXR range from 3 to 100 keV and increases to ~ 5 – 10 keV in the γ -ray range up to 17 MeV. For all *RHESSI* spectral analysis presented in this paper, the SPEX procedure (Schwartz et al. 2002) was used.

The combination of high spatial and spectral resolution over a broad energy range (covering “thermal” and “nonthermal” X-rays), the high time resolution, and the high sensitivity and dynamic range (achieved by a system of two attenuators that can be brought into the field of view when the count rate is too high) make *RHESSI* uniquely capable of studying the NE and its relevance for the flare energetics. *RHESSI*'s combined hard-soft (down to 3 keV) X-ray observations with a high spectral resolution of 1 keV provide us with the possibility of trying to determine the low cutoff energy E_1 from the spectral transition from thermal to nonthermal bremsstrahlung, as suggested by Holman & Benka (1992) and Benka & Holman (1994); for recent applications of this concept to *RHESSI* spectra, see Holman (2003), Holman et al. (2003), and L. Sui et al. (2005, in preparation). In this paper we make use of this capability in order to get a second, independent approach to the beam low cutoff energy in addition to the TNE analysis. If both approaches yield similar estimates for E_1 , this would give us some confidence on the derived values.

RHESSI also provides us with the unprecedented capability of doing X-ray imaging spectroscopy (e.g., as performed by Emslie et al. [2003] for the large X-class flare of 2002 July 23). Exploring *RHESSI*'s imaging spectroscopy capabilities, however, is beyond the scope of this paper.

4. DATA SELECTION AND ANALYSIS

The selection of events was based on the demands that (1) the overall impulsive flare phase was covered by *RHESSI* observations (i.e., not interrupted by *RHESSI* nighttime or the passage of the spacecraft through the South Atlantic Anomaly), (2) up to at least 40 keV emission above the background level was observed during the impulsive phase (to ensure an accurate determination of $F_1(t)$ and $\delta(t)$ for the whole time series), and (3) the reconstructed images provide us with insight into the source geometry and size.

Table 1 lists the characteristics of the four events selected for the analysis: the start and end times (which refer to the 12–25 keV emission observed by *RHESSI*), the *GOES* class, the heliographic position measured from *RHESSI* images, the area A of the footpoints seen in HXR, the loop length l inferred from the footpoint separation, the derived volume $V = Al$ of the hot loop, the peak emission measure EM_p and peak temperature T_p derived from *GOES* and *RHESSI* (*RHESSI* values are listed inside parentheses), and the peak of the beam power in electrons ≥ 25 keV, $P_{25,p}$. All four events show some ENE when we compare the *RHESSI* 25–100 keV light curve and the time derivative of the *GOES* 1–8 Å flux.

For *RHESSI* image reconstruction, the CLEAN and *pixon* methods were used (Hurford et al. 2002). To estimate the footpoint areas, we counted the pixels within the 50% contour level of the brighter footpoint in the 25–50 keV images reconstructed with *pixon* using *RHESSI* grids 3–8 (giving an angular resolution of $\sim 7''$). The separation of the footpoints was measured from the centroids of both footpoints and corrected for foreshortening. We note that in these events the footpoints are unresolved in the grids; thus, our areas are upper limits.

For each flare we evaluated spatially integrated HXR spectra summed over consecutive 4 s intervals to derive the electron beam power as a function of time. In order to avoid the effects of the rapid modulation of the count rates caused by the grids, the integration time was chosen to correspond roughly to the spin

TABLE 1
SELECTED EVENTS

Date	Start (UT)	End (UT)	Class	Location (deg)	A (10^{16} cm 2)	l (10^8 cm)	V (10^{26} cm 3)	EM_p (10^{49} cm $^{-3}$)	T_p (MK)	$P_{25,p}$ (10^{27} ergs s $^{-1}$)
2002 Feb 20.....	11:04:08	11:12:20	C7.5	N14 W73	26.2	34.5	9.0	0.7 (0.6)	15.0 (20.3)	7.4
2002 Apr 14.....	23:59:32	00:25:08	M3.2	N20 W59	19.1	45.0	8.6	4.0 (3.2)	17.9 (21.2)	20.9
2002 Apr 15.....	23:08:56	23:20:48	M1.2	N20 W72	21.5	77.3	16.7	1.3 (1.2)	17.0 (19.7)	6.7
2002 Jun 2.....	11:44:04	11:49:48	M1.0	S19 E10	20.6	16.8	3.4	1.2 (1.0)	15.6 (18.0)	4.5

period of the *RHESSI* spacecraft (~ 4 s). The photon spectra were derived with 1 keV energy bins using all front detector segments except 2 and 7 (which have lower spectral resolution and high threshold energies) and deconvolved with the full detector response matrix, i.e., including off-diagonal elements (see Smith et al. 2002). In all four events, the *RHESSI* thin attenuators were in the detector's field of view (attenuator state A1) throughout, limiting the lower energy of the X-ray observations to ~ 6 keV. For background subtraction, a linear interpolation between the count rate spectra before and after the flare has been applied and subtracted from the observed flare count spectra for each 4 s interval.

Spectral fits were obtained using a forward-fitting technique for which the functional form of the incident photon flux spectra is assumed for a parametric model of the source. Specifically, we used the line and continuum spectrum of an isothermal plasma based on the MEKAL code in the *RHESSI* spectral software plus the thick-target bremsstrahlung spectrum computed from a power-law electron injection with a low energy cutoff (see Holman 2003). This gives five free parameters. This function is folded through the instrument response (for attenuator state A1) to provide the expected count rates. The free parameters are varied until a minimum χ^2 fit to the count rates is obtained. The error on a parameter can be estimated by finding the range over which χ^2 remains acceptable. Poisson statistics were assumed plus a 5% systematic uncertainty on every measured count rate. In the bremsstrahlung computations, the Haug (1997) relativistic bremsstrahlung cross section with the Elwert (1939) correction was used.

Emission measure and temperature were derived from *GOES* 0.5–4 and 1–8 Å observations (e.g., Thomas et al. 1985; Garcia 1994) with a time cadence of 3 s as well as from the *RHESSI* 4 s integration spectral fits. In Table 1 we list the peak EM and peak T derived from *GOES* and *RHESSI* for each flare. As can be seen from the table (as well as in Fig. 7, discussed further in § 5.2), *RHESSI* gives systematically higher temperatures and smaller EMs (a finding that is in accordance with other *RHESSI* studies; e.g., L. Sui et al. 2005, in preparation). This might be an indication of a multithermal flare plasma. On the other hand, the difference could also be the result of calibration errors and model dependences. In the following we use the *GOES* $EM(t)$ and $T(t)$ for the derivation of the thermal plasma parameters as a function of time, but the *RHESSI* values are similar.

It should be noted that in the *RHESSI* and *GOES* analysis software, the MEKAL atomic model describing the thermal X-ray spectrum of a solar flare (Mewe et al. 1985) is used. This is significantly different from the CHIANTI atomic model with solar coronal abundances and recent ionization equilibrium ion fractions (ver. 4.2; see Young et al. 2003). The differences are likely to be the result of the different element abundances (Mewe et al. use cosmic abundances) and ion fractions (Phillips 2004). In a recent paper (White et al. 2004), the differences between the MEKAL and CHIANTI models in deriving EM and tem-

perature from *GOES* observations are investigated. On average, the derived temperatures using the CHIANTI model with coronal abundances are ~ 1 –2 MK higher and the EMs up to a factor of 4 smaller than those of the MEKAL model. This means that at the moment there is uncertainty in the derivation of thermal plasma parameters from SXR data such as *GOES* and *RHESSI*. However, the uncertainty is essentially a constant factor in the inferred EM value and would not affect the light-curve shapes.

5. RESULTS

5.1. 2002 February 20 Flare

The C7.5 flare of 2002 February 20, 11:04 UT, was one of the first flares observed by *RHESSI*, and different aspects of it have already been reported in a number of papers (Aschwanden et al. 2002; Krucker & Lin 2002; Sui et al. 2002; Vilmer et al. 2002). Figure 1 shows an image of the flare reconstructed with the *pixion* algorithm at the maximum of the nonthermal emission (integration time is 13 s; i.e., three rotations of the *RHESSI* spacecraft). The 25–50 keV image reveals two distinct footpoints and a faint loop-top source. At 6–12 keV, a second, smaller loop system is most likely revealed.

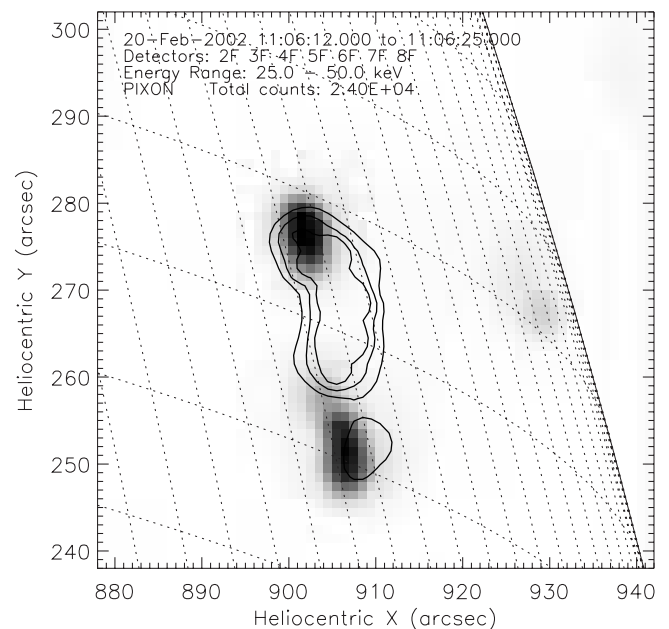


FIG. 1.—Flare of 2002 February 20. The gray-scale image represents the 25–50 keV *RHESSI* image reconstructed with *pixion* using front detector segments 2–8 during the maximum of the hard 25–50 keV emission. The contour lines indicate the corresponding soft 6–12 keV image (obtained with front detector segments 1, 3, 4, 5, 6, and 8). Contours are drawn at 12%, 20%, and 30% levels of the maximum intensity. The solid line denotes the solar limb, and the dotted lines denote a heliographic grid. [See the electronic edition of the *Journal* for a color version of this figure.]

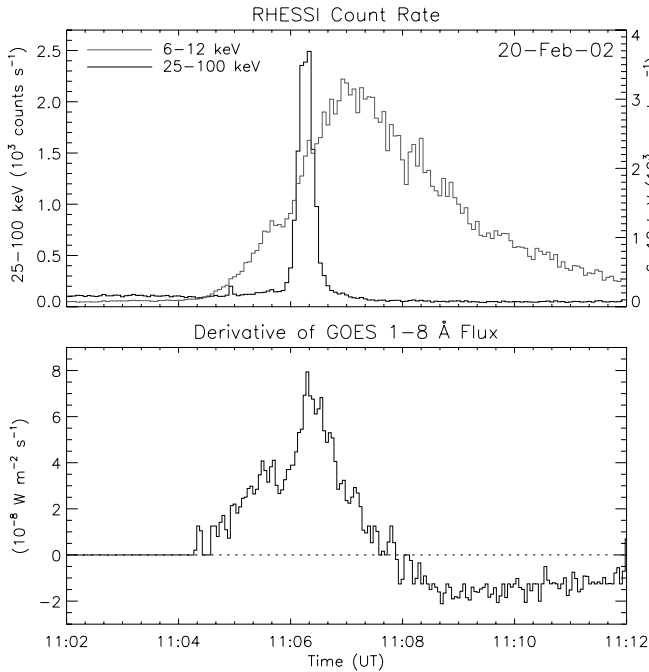


FIG. 2.—*RHESSI* count rates (4 s data) in two energy bands (6–12 and 25–100 keV) summed through front detector segments 1–9 (excluding 2 and 7) and time derivative of the *GOES* 1–8 Å flux (3 s data) for the 2002 February 20 flare.

Figure 2 shows the *RHESSI* count rates in the 6–12 and 25–100 keV energy bands together with the time derivative of the *GOES* 1–8 Å flux, illustrating the ENE. The flare is characterized by quite flat HXR spectra (at the peak, $\delta = 3.9$) and shows a clear soft-hard-soft spectral evolution. The maximum temperatures derived from *GOES* and *RHESSI* are 15 and 20 MK, respectively. The energy E_{loop} of electrons stopped above the transition zone increases from about 15 to 35 keV during the flare (see Fig. 3, left panel). For a specific low cutoff energy E_1 , the fraction of the injected beam power that goes into the hot part of the loop is determined by E_{loop} and δ . Figure 3 (right panel) shows the evolution of the beam power that goes into the hot loop together with the total injected beam power for $E_1 = 20$ keV.

In Figure 4 the outcome of the TNE analysis is shown. We plot the range of actual power required to explain the SXR flux, $P_{\text{in}}(t)$, together with the beam power that goes into the loop

above the transition zone, $P_{\text{beam}}(t)$, for increasing values of the low cutoff energy E_1 . The figure reveals that even for this flat spectrum the beam power is strongly dependent on the low cutoff energy, as expected (Brown 1971). To match the total SXR plasma energy content (also accounting for cooling losses) and that in the electron beam—i.e., the cumulative integrals of the plotted $P_{\text{in}}(t)$ and $P_{\text{beam}}(t)$ curves— E_1 should be in the range $18 \text{ keV} \lesssim E_1 \lesssim 21 \text{ keV}$. We can compare this E_1 derived from the TNE analysis with that derived from the *RHESSI* spectral fits applied to consecutive 4 s intervals handling E_1 as a free fit parameter. Minimizing χ^2 in each individual 4 s spectral fit, we find an event-averaged low cutoff energy in the range $17 \text{ keV} \lesssim E_1 \lesssim 21 \text{ keV}$. This means, with both approaches (TNE analysis and spectral fitting), that we come to the same estimate for E_1 . However, it is obvious from the plots in Figure 4 that no constant choice of E_1 yields a reasonable time correlation match between the time variations in $P_{\text{in}}(t)$ and $P_{\text{beam}}(t)$. If our assumptions were right, we would expect that the derived $P_{\text{beam}}(t)$ curve should at least lie within the generously estimated minimum-maximum range of $P_{\text{in}}(t)$ during the whole impulsive phase. We later discuss the effect of allowing E_1 to vary with time.

5.2. 2002 April 14 Flare

The M3.2 flare that occurred on 2002 April 14, 23:59 UT, was a gradual event with nonthermal emission for more than 15 minutes (see the 25–100 keV light curve in Fig. 5). The source of the emission is concentrated along the loop top, and only faint footpoint emission is detectable. For a short interval at the highest peak (which occurs late in the event), emission along the whole loop down to the footpoints is visible at 25–50 keV at 00:10:22 UT (Fig. 6).

In Figure 7 we show the resulting hot loop plasma and electron beam parameters derived from the *GOES* and *RHESSI* observations (the *GOES* data have been smoothed with a 30 s boxcar average). In Figure 7a the temperature evolution is plotted showing a double peak; the maximum temperatures observed by *GOES* and *RHESSI* are 18 and 21 MK, respectively. In Figure 7b the evolution of the EM as derived from *GOES* and *RHESSI* data is plotted. Figure 7c shows the rate of change of the thermal energy estimates $U_{\text{th}}(t) = 3n(t)VkT(t)$ and $U_{\text{th}}(t) = 5n(t)VkT(t)$, respectively. In Figure 7d the derived radiative and conductive cooling losses are plotted. It is worth noting that radiative cooling becomes important mainly after the impulsive

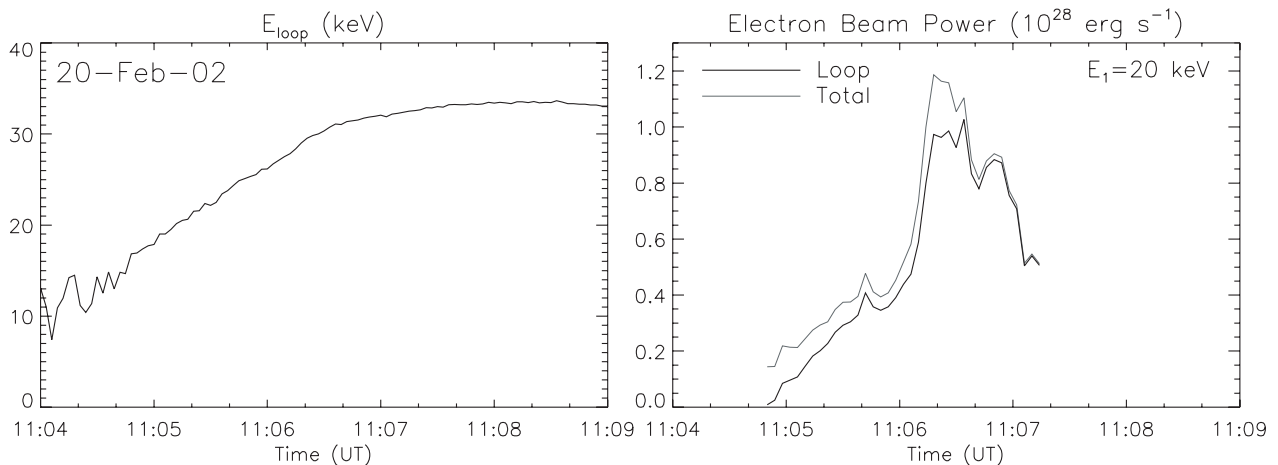


FIG. 3.—Flare of 2002 February 20. Left panel: Evolution of the energy E_{loop} of electrons stopped above the transition zone. Right panel: Total electron beam power injected (thin line) together with that part of the beam power that goes into the loop above the transition zone (thick line) for $E_1 = 20$ keV.

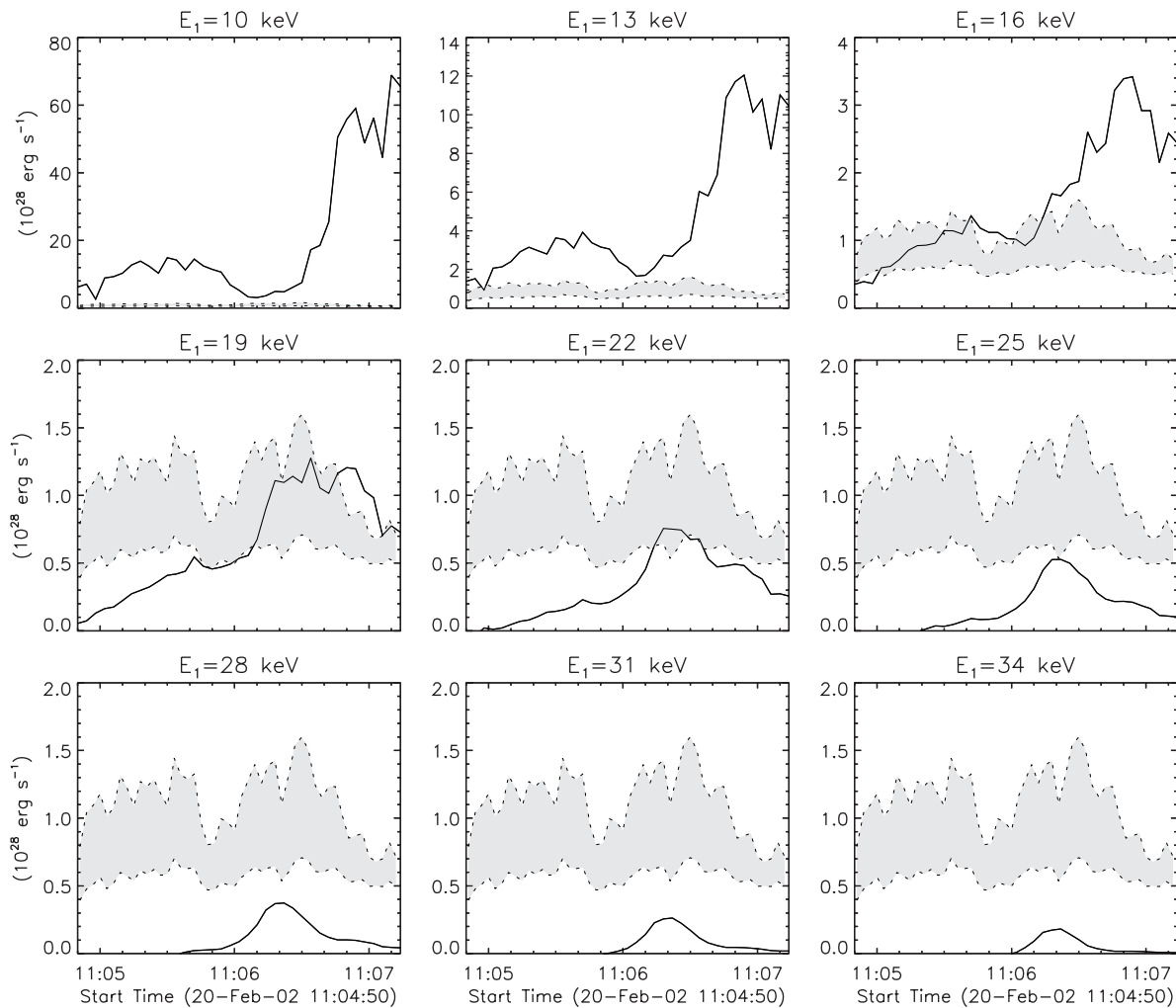


FIG. 4.—Flare of 2002 February 20. Comparison of the actual power $P_{\text{in}}(t)$ required to explain the observed SXR flux (minimum-maximum range; shaded area) and the electron beam power $P_{\text{beam}}(t)$ that goes into the hot part of the loop (solid line), calculated for different low cutoff energies E_1 .

phase, whereas losses by conductive cooling may be a larger factor during the impulsive phase than the thermal power actually observed (see Figs. 7c and 7d), at least in the classical limit used (for a detailed observational study on flare plasma cooling, see, e.g., Aschwanden & Alexander 2001).

Figures 7e and 7f show the electron flux at 50 keV and the electron spectral index as a function of time, respectively; these are distinctly anticorrelated (i.e., show a soft-hard-soft evolution on very short timescales). The event is characterized by steep HXR spectra, $\delta \gtrsim 6.7$. In Figure 7g we plot $E_{\text{loop}}(t)$, which is extremely high due to the high loop column densities (up to $4.9 \times 10^{20} \text{ cm}^{-2}$). At the onset of the impulsive phase, E_{loop} is already as high as 35 keV and increases to 61 keV during the event. In Figure 7h the injected electron beam power together with the fraction that goes into the loop is plotted.

To match the total SXR plasma energy content and the beam energy in this event, the low cutoff energy should be in the range $26 \text{ keV} \lesssim E_1 \lesssim 29 \text{ keV}$ (see Fig. 8). Because of the steep spectra, the calculated beam power here is extremely sensitive to the low cutoff energy. Furthermore, the high E_{loop} and steep spectra mean that almost all of the injected beam power goes into the loop above the transition zone (see Fig. 7h). Thus, most of the accelerated electrons are stopped within the loop, and only a very small fraction reaches the chromosphere. We note that $\phi \geq 0.9$ throughout. This finding is consistent with the

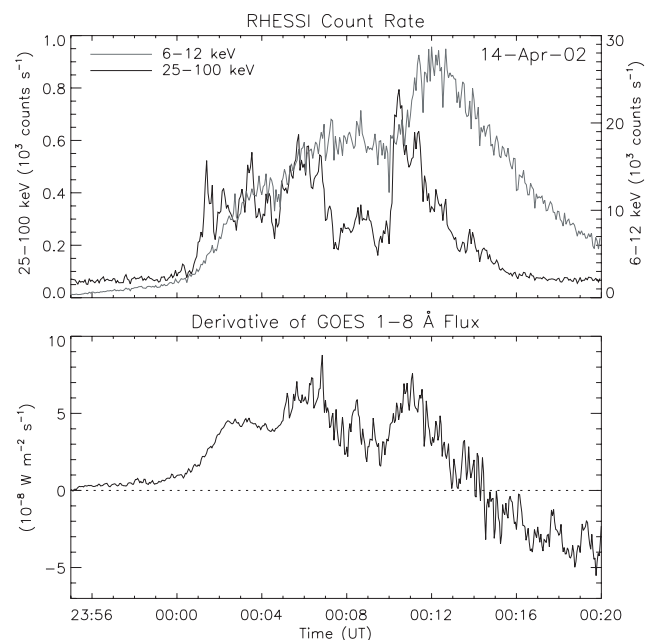


FIG. 5.—*RHESSI* count rates in two energy bands (6–12 and 25–100 keV) and time derivative of the *GOES* 1–8 Å flux for the 2002 April 14 flare. *GOES* data are smoothed with a 30 s boxcar average.

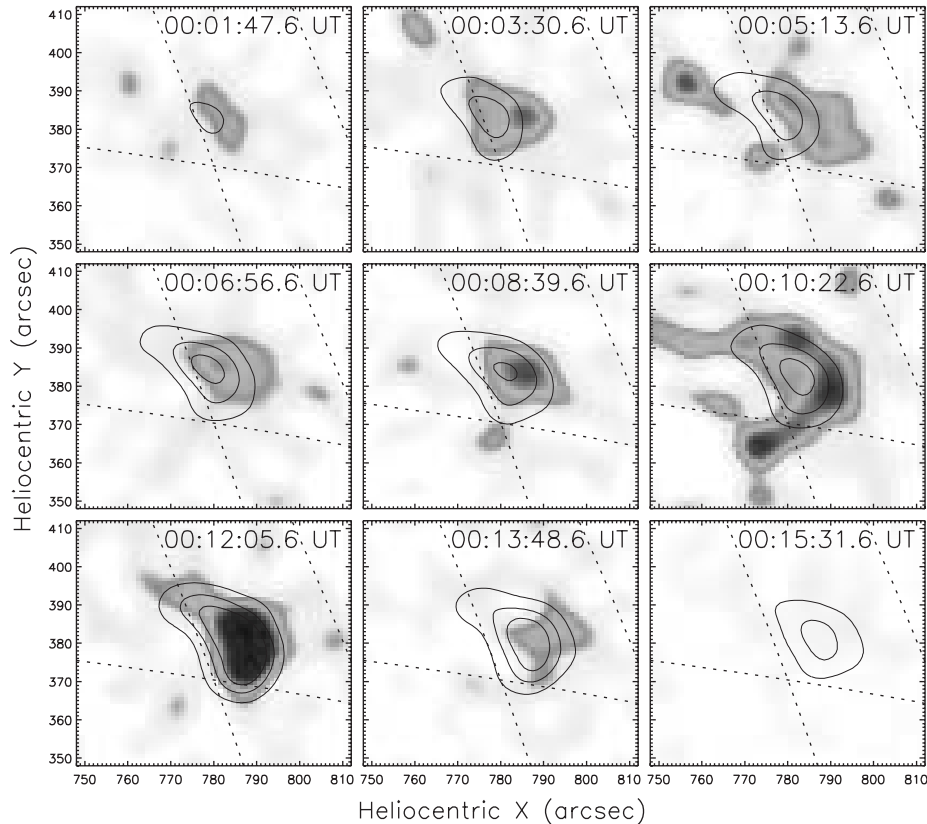


FIG. 6.—Flare of 2002 April 14. Time series of 25–50 keV *RHESSI* images reconstructed with CLEAN integrating through front detector segments 3–8 over five *RHESSI* spin periods (20.6 s). Contours indicate the corresponding images at 6–12 keV obtained with front detector segments 3–8, except 7 (levels are 20%, 40%, and 60%). Start times of consecutive images are separated by 103 s. Images and contour levels are normalized to the respective maxima of the time series. The dotted lines denote a heliographic grid. [See the electronic edition of the *Journal* for a color version of this figure.]

reconstructed images in which the emission comes mainly from the loop top and within the loop; only weak footpoint emission is seen. Thus, this is an unusual case in which HXR emission is almost entirely coronal, the loop-top region being itself a thick target (see Veronig & Brown 2004). Note that such an event, in which the HXR emission is predominantly coronal, was already reported from *Yohkoh* observations (Kosugi et al. 1994).

From Figure 8 it can be seen that for $E_1 = 28$ keV, the time profiles of $P_{\text{in}}(t)$ and $P_{\text{beam}}(t)$ do show some agreement. However, the TNE power time correlation across the event is no better than that for the ENE SXR-HXR fluxes, $r = 0.7$. The event-averaged low cutoff energy derived from the spectral fits yields $18 \text{ keV} \lesssim E_1 \lesssim 21 \text{ keV}$, i.e., a value that is outside the range of our TNE argument (there would be far too much power in the beam; see Fig. 8), possibly because of the plasma being far from isothermal (see discussion). (Note that the discrepancy may be increased when the CHIANTI model is used instead of the MEKAL thermal model.)

In this event E_{loop} is very large, so most of the beam electrons lose all their energy in the corona. Thus, evaporation is not driven directly by the beam; rather, the beam heats the corona, and then evaporation is driven by thermal conduction. The observed column densities are too large for beam-driven evaporation but are in good agreement with conductive evaporation (see Veronig & Brown 2004).

5.3. 2002 April 15 Flare

The M1.2 flare of 2002 April 15, 23:08 UT, took place in the same active region (NOAA AR 9901) near the northwest limb as

the 2002 April 14 event and has similar overall characteristics. Nonthermal emission is observed for about 10 minutes (see the 25–100 keV light curve in Fig. 9). Figure 10 shows *RHESSI* images in the 25–50 and 6–12 keV energy bands obtained at the maximum of the flare. Emission from two footpoints and from within the loop is seen at 25–50 keV; the 6–12 keV emission is mainly from within the loop. In a recent paper on this flare, Sui & Holman (2003) report evidence of the formation of a large-scale, reconnecting current sheet between the flare loop top and a coronal source above the loop top (this source is also seen in Fig. 10). Furthermore, for this and the 2002 April 14 flare, altitude variations of the loop-top source that initially moved downward and then upward have been reported (Sui et al. 2004).

The peak temperatures derived from *GOES* and *RHESSI* are 17 and 20 MK, respectively. The loop column density reaches a maximum of $3.5 \times 10^{20} \text{ cm}^{-2}$, which corresponds to $E_{\text{loop}} = 52$ keV (for the time evolution, see Fig. 11, *left panel*). *RHESSI* spectroscopy reveals steep HXR spectra (minimum $\delta = 5.9$). As in the 2002 April 14 flare, because of the high column densities and steep spectra most of the beam power goes into the loop (see Fig. 11, *right panel*); $\phi \geq 0.9$ throughout the event.

To match the total energy in the SXR plasma and the electron beam, the low cutoff energy should be in the range $23 \text{ keV} \lesssim E_1 \lesssim 26 \text{ keV}$ (see Fig. 12). As can be seen in the figure, for $E_1 = 25$ keV, $P_{\text{in}}(t)$ and $P_{\text{beam}}(t)$ can be matched quite well except during the first ~ 100 s, when $P_{\text{beam}}(t)$ is too low and does not lie within the extreme range of $P_{\text{in}}(t)$. However, during this interval the determination of the beam power is quite uncertain

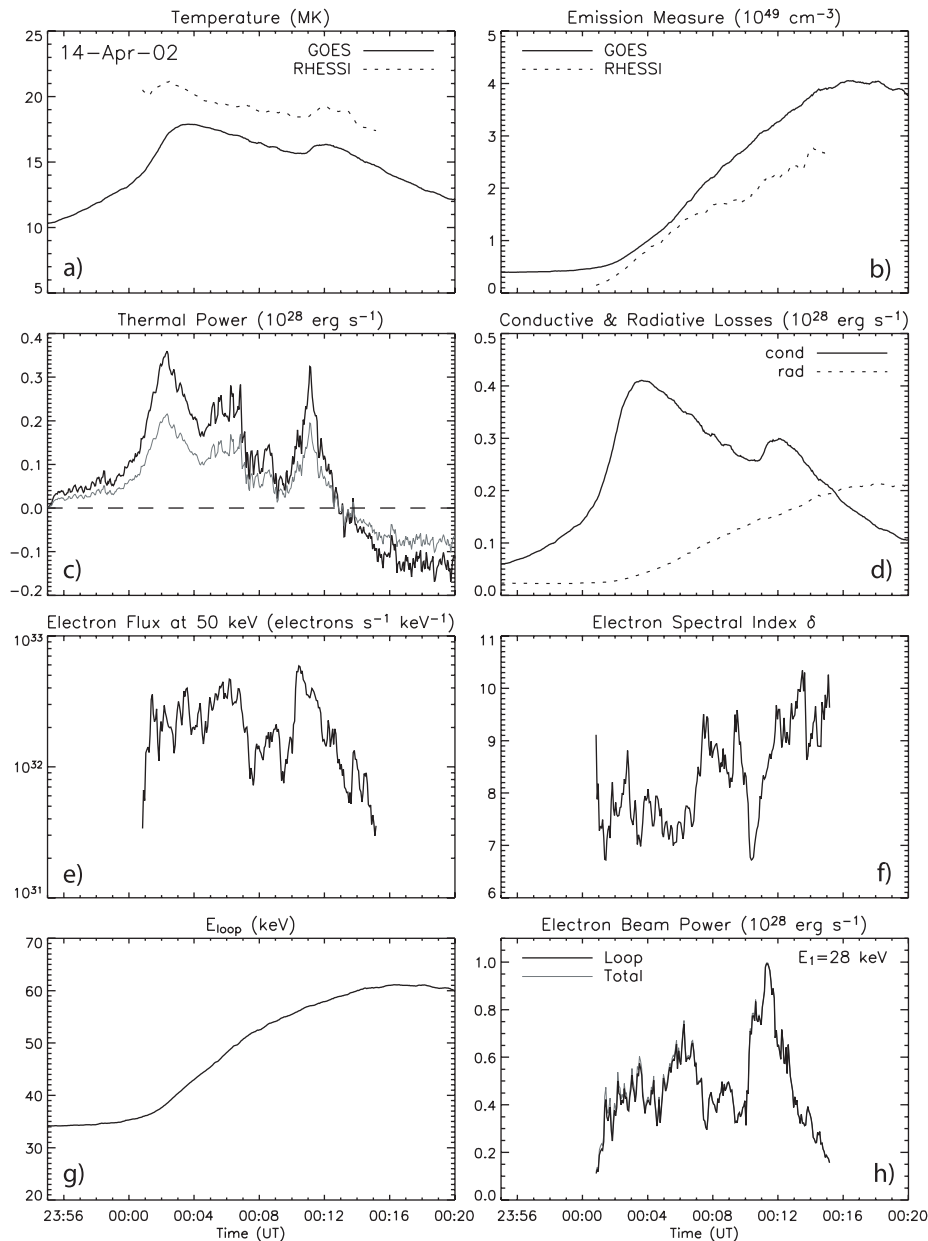


FIG. 7.—Flare of 2002 April 14. Evolution of various hot loop plasma and electron beam parameters derived from SXR and HXR observations. For detailed description, see the text (§ 5.2).

because of the small fluxes and very steep spectra ($10 \lesssim \delta \lesssim 12$). The steep spectra are also the reason for the extremely high beam power calculated for low cutoff energies $E_1 \lesssim 16$ keV (see Fig. 12).

The isothermal plus cutoff power-law spectral fits yield values for the low cutoff energy in the range $17 \text{ keV} \lesssim E_1 \lesssim 20 \text{ keV}$, again somewhat below the 25 ± 2 keV derived from the TNE analysis and possibly due to multithermality. A sample *RHESSI* spectrum together with the thermal and nonthermal bremsstrahlung fits is shown in Figure 13.

5.4. 2002 June 2 Flare

The M1.0 flare of 2002 June 2, 11:44 UT, is characterized by a short impulsive phase ($\lesssim 2$ minutes) with a double peak structure. It shows the Neupert light-curve effect for the two impulsive peaks, but strong deviations from it occur afterward

(Fig. 14). The hard 25–50 keV emission is concentrated in two footpoints. At the very beginning the soft 6–12 keV images also show impulsive footpoint emission, whereas afterward the 6–12 keV emission originates from between the footpoints, indicating that the source region is near the loop top (Fig. 15). From *Yohkoh* observations, Hudson et al. (1994) reported impulsive SXR footpoint emission that closely matched the HXR time profile demonstrating chromospheric heating on short time-scales during the interval of nonthermal energy release. In the *RHESSI* observations of the 2002 June 2 flare (see Fig. 15), we can directly observe the transition of SXR from impulsive footpoint emission to coronal loop emission. The peak temperatures derived from *GOES* and *RHESSI* observations are 16 and 18 MK, respectively.

The HXR spectra are flat (minimum $\delta = 3.8$). Here E_{loop} is very small (9 keV) at the onset of the event and increases during

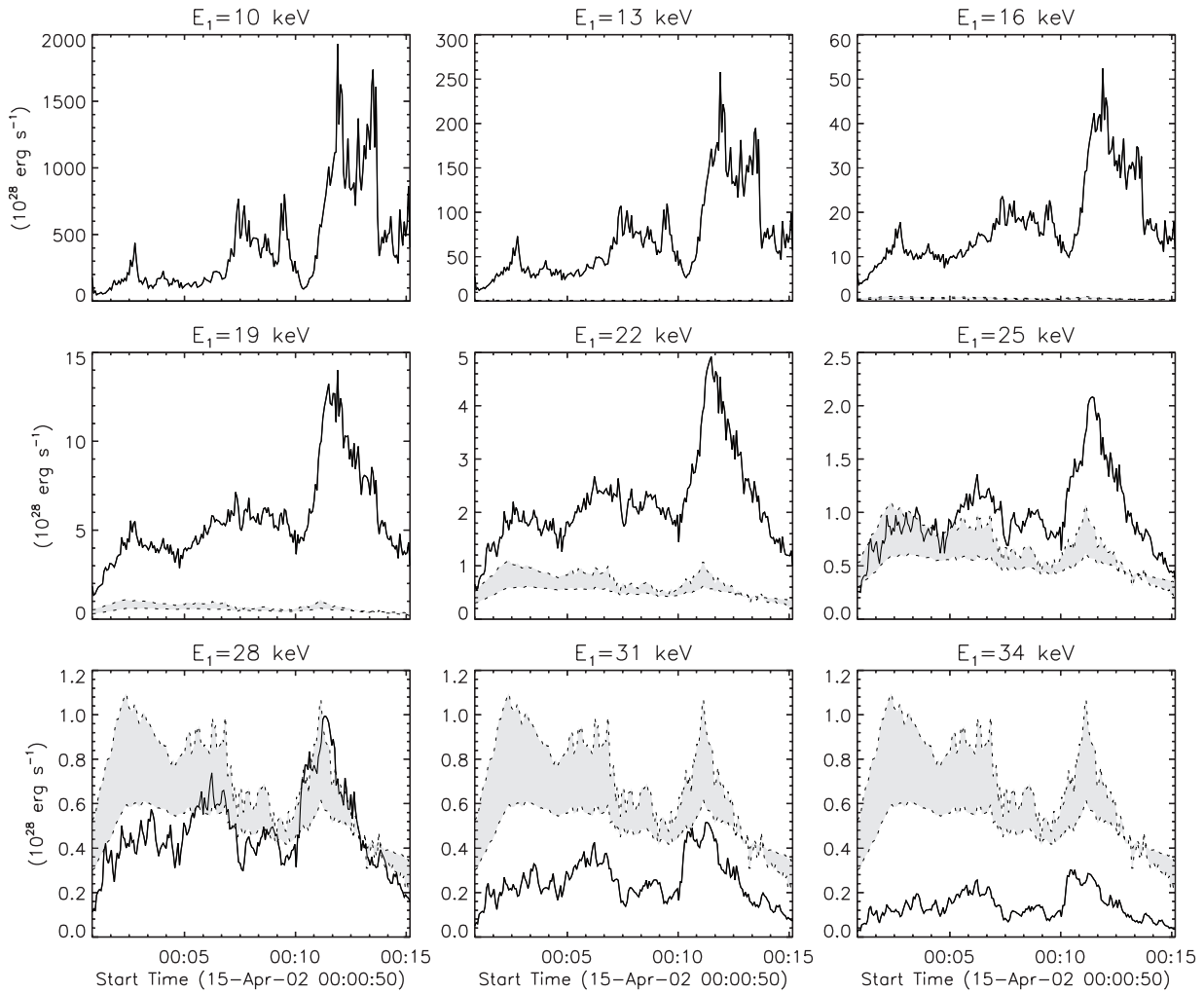


FIG. 8.—Same as Fig. 4, but for the 2002 April 14 flare.

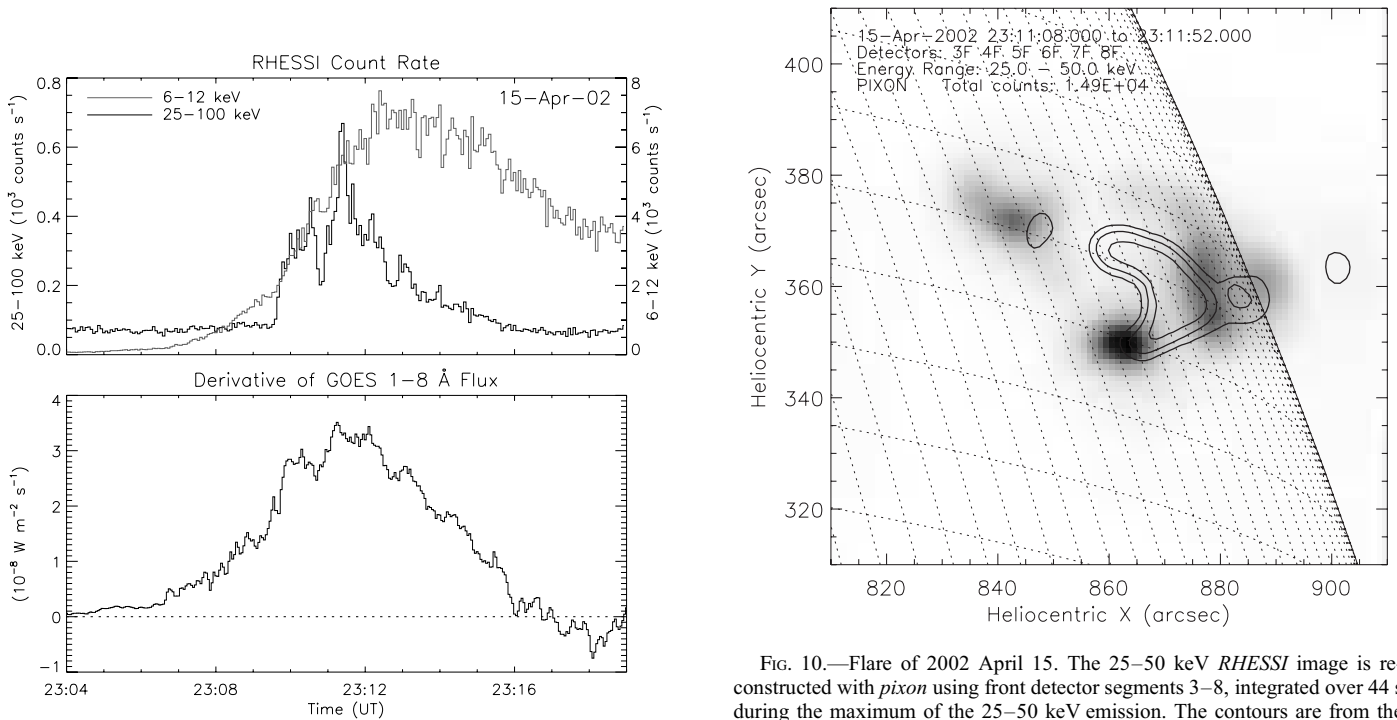


FIG. 9.—*RHESSI* count rates in two energy bands (6–12 and 25–100 keV) and time derivative of the *GOES* 1–8 Å flux for the 2002 April 15 flare. *GOES* data are smoothed with a 30 s boxcar average.

FIG. 10.—Flare of 2002 April 15. The 25–50 keV *RHESSI* image is reconstructed with *pixion* using front detector segments 3–8, integrated over 44 s during the maximum of the 25–50 keV emission. The contours are from the corresponding 6–12 keV image using front detector segments 3–8, except 7 (levels are 10%, 20%, and 40% of the peak flux). The solid line denotes the solar limb, and the dotted lines denote a heliographic grid. [See the electronic edition of the *Journal* for a color version of this figure.]

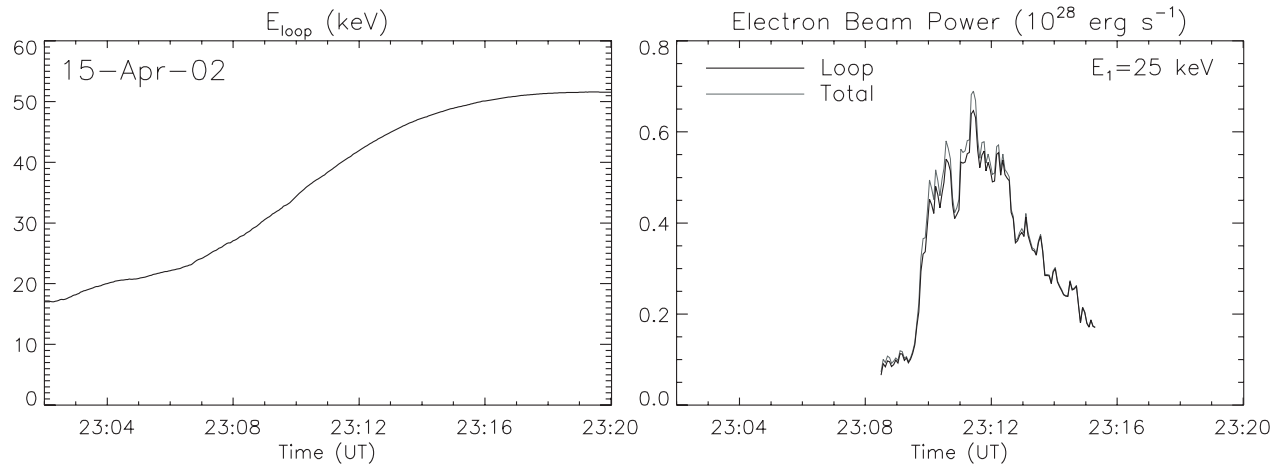


FIG. 11.—Same as Fig. 3, but for the 2002 April 15 flare.

the flare up to 34 keV (Fig. 16). The sharp increase of E_{loop} starting at 11:44 UT coincides well with the beginning of the impulsive HXR emission, indicating explosive electron beam-driven evaporation. The extremely low E_{loop} at the very beginning of the impulsive phase (“empty loop”) is consistent with *RHESSI* images showing that during these times the 6–12 keV

emission originates from footpoints, and only later—after the loop is filled with evaporated chromospheric matter and dense enough to collisionally stop these low-energy electrons—is it from the loop top.

To match P_{in} and P_{beam} (in terms of total energies), the low cutoff energy should be in the range $12 \text{ keV} \lesssim E_1 \lesssim 18 \text{ keV}$. The

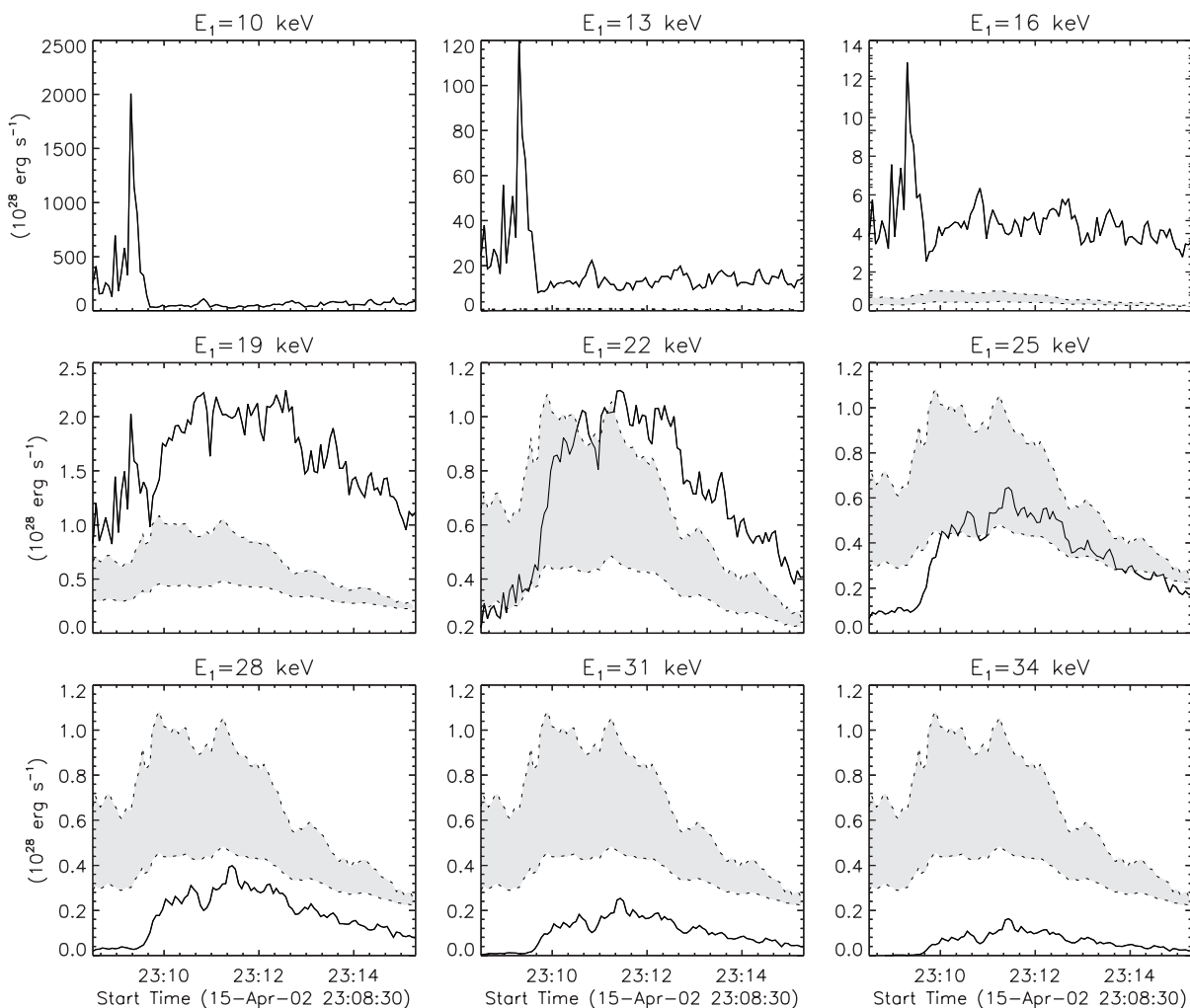


FIG. 12.—Same as Fig. 4, but for the 2002 April 15 flare.

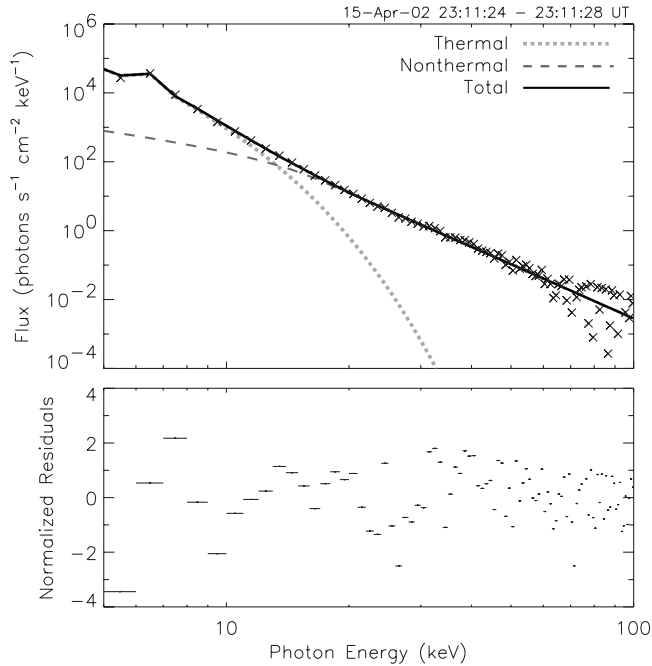


FIG. 13.—*Top panel:* *RHESSI* background-subtracted, spatially integrated photon spectrum (*crosses*) derived for a 4 s interval at the maximum of the nonthermal emission of the 2002 April 15 flare. Also shown is the best-fit photon spectrum made up of two components. The dotted curve shows the spectrum from an isothermal plasma. The dashed curve shows the nonthermal thick-target bremsstrahlung spectrum from an electron beam with a power-law distribution at energies above $E_1 = 17$ keV. The solid line represents the sum of both components. *Bottom panel:* Residuals, defined as the observed flux minus the model flux divided by the estimated 1σ uncertainty (including random Poisson statistics plus a 5% systematic uncertainty) in each data point. [See the electronic edition of the *Journal* for a color version of this figure.]

time histories of $P_{\text{in}}(t)$ and $P_{\text{beam}}(t)$ do show some agreement for the two impulsive peaks but not afterward (see Fig. 17).

6. DISCUSSION AND CONCLUSIONS

6.1. General Remarks

On the basis of the assumption of a monolithic single-loop structure consistent with *RHESSI* images and most previous flare modeling, and on a simple upper-lower bound estimate of terms in the energy-hydrodynamic equations, we have found that analysis of Neupert effect (NE) data, including source physics, does *not* lead to a better temporal correlation of beam input and plasma heating power than that of the raw HXR-SXR flux data, unless the beam low energy cutoff is allowed to vary with time. If we accepted the geometric assumptions and believed in the beam-heating interpretation of impulsive phase NE, we would then have powerful means of determining not only the low-energy beam cutoff but also its time variation, which could be a valuable diagnostic for acceleration models. (This is, of course, a restatement, in more optimistic terms, of the long-known fact that beam power is very sensitive to the low energy cutoff; e.g., Neupert 1968; Brown 1971; Hudson 1972; Hoyng et al. 1976; Lin & Hudson 1976.) The fact that the values of E_1 obtained from the energy balance argument are somewhat higher than those inferred from HXR spectral fitting with an isothermal plasma plus power-law beam component could be seen either as a failure of the model or as an argument to consider a possible multithermal plasma spectral contribution (e.g., Brown 1974; Piana et al. 1995), as suggested by the higher T from *RHESSI* than from *GOES*. However, there are several issues and alter-

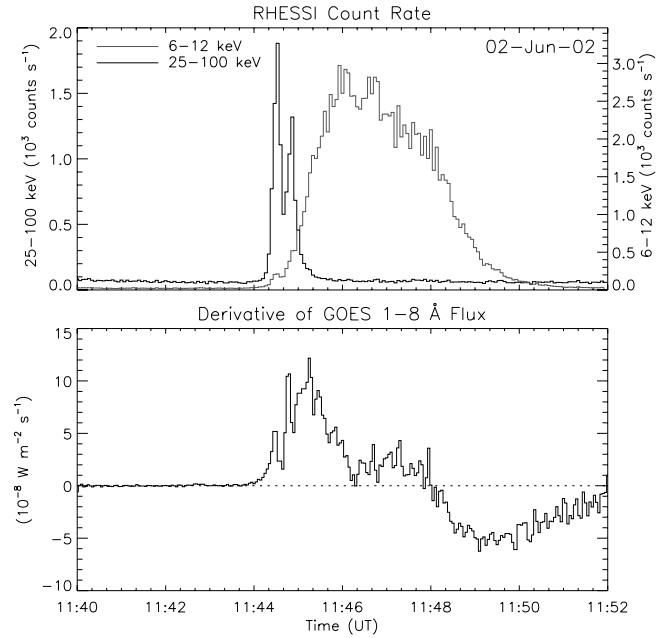


FIG. 14.—*RHESSI* count rates in two energy bands (6–12 and 25–100 keV) and time derivative of the *GOES* 1–8 Å flux for the 2002 June 2 flare.

native scenarios that need to be thoroughly explored before these conclusions can really be taken seriously. Among these are the following:

1. uncertain values of geometric and thermal parameters, including multithermality;
2. spatial fine structure in the loop;
3. noncollisional beam energy losses;
4. additional (nonbeam) heating processes;
5. time variation of E_1 ;
6. flaws in the energy budget model; and
7. time-dependent fine structure within the loop.

6.2. Uncertain Values of Geometric and Thermal Parameters

The footpoint separation and thus the loop length can be quite accurately measured from the *RHESSI* images. However, the footpoint area (and, as a consequence, the volume estimate) is much more uncertain, as it depends on the image reconstruction method, the *RHESSI* grids used, the time interval selected, and the method for measuring the area. It is worth noting that for a very simple single source, Schmahel & Hurford (2002) developed a method for determining the source size from *RHESSI* images based directly on the modulation profiles instead of the mapped images. The footpoint areas listed in Table 1 are all basically consistent with the minimum area that can be resolved by the collimators used (the finest *RHESSI* grid used was grid 3, which gives an angular resolution of $\sim 7''$). Thus, these areas represent upper limits to the real ones. However, for the present analysis, changing the geometric parameters does not substantially alter the main results, which we checked by enhancing/reducing the determined areas by up to a factor of 3. This basically shifts the power curves up/down by a scale factor, changing the E_1 needed for a mean power match but not improving the temporal correlation of the power profiles, unless one allows time variations in the area and length. In reconnection models as well, the volume is expected to change with time, since higher and higher loops are formed that are presumably longer and with greater volume, a fact supported by observations. However, in

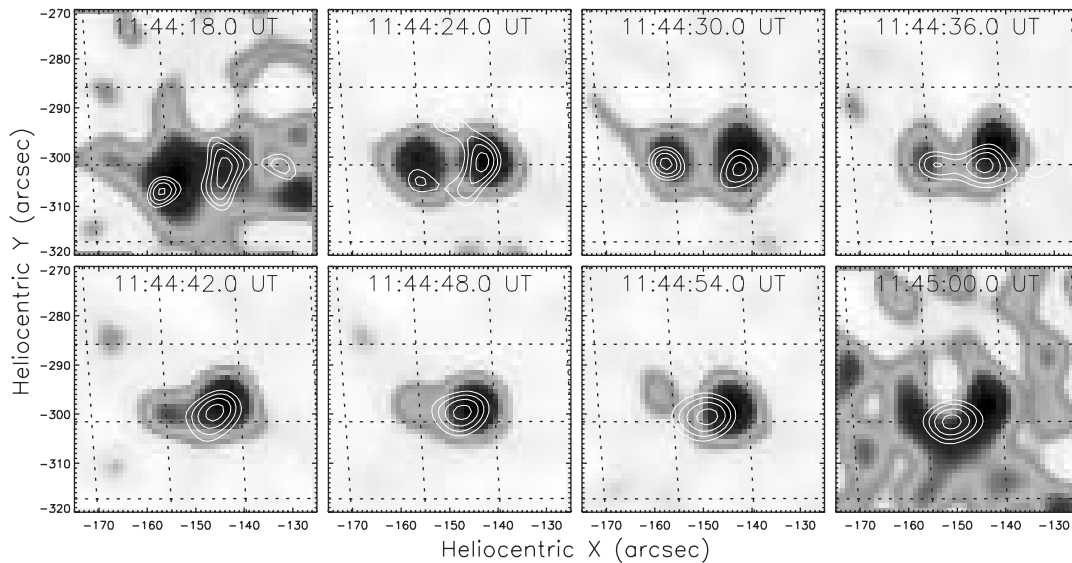


FIG. 15.—Flare of 2002 June 2. Time series of 25–50 keV images obtained with CLEAN integrating 12 s through front detector segments 3–8 (each image is scaled separately). Contour levels (at 65%, 75%, 85%, and 95% of the peak flux of each image) indicate the corresponding 6–12 keV images obtained with front detector segments 3–8, except 7. The dotted lines denote a heliographic grid. [See the electronic edition of the *Journal* for a color version of this figure.]

order to improve the temporal correlation, the geometric parameters would have to have nonmonotonic temporal evolution.

A further source of uncertainty is the determination of temperature and EM of the thermal source as inferred from the *GOES* and *RHESSI* SXR observations. These constitute model dependences (e.g., multithermality) as well as calibration errors (discussed in detail in § 4).

In part of equation (18), to get analytic expressions we have neglected electron collisional pitch angle increase with depth N . However, this effect typically only shifts N values by a factor of $\leq 3/2$ (Brown 1972; Emslie 1978), which is well within the uncertainty of our other approximations. A more serious effect neglected here (and throughout most of the literature) could be that of magnetic field convergence and electron mirroring. This would increase ϕ and shift our power light curves but, unless it is time-dependent, would not improve the theoretical Neupert effect (TNE) cross-correlation in time.

6.3. Spatial Fine Structure in the Loop

When the loop filling factor f is smaller than 1, the calculated thermal energy is decreased by \sqrt{f} , as is the conducted

power, since the area is reduced (if f is filamentary) but the temperature gradient is fixed by T . The radiated power is unaffected, since it uses the observed emission measure (EM). The overall effect is to change the relative scale of some of the coefficients in the energy equation. Repeating the TNE analysis assuming $f = 0.1$, the low cutoff energies derived from the TNE analysis changed by only $\lesssim 3$ keV with regard to the main analysis based on $f = 1$. The $P_{\text{in}}(t)$, $P_{\text{beam}}(t)$ correlation might be better if we allowed $f = f(t)$. This is physically possible, although in order to shift the $P_{\text{in}}(t)$ and $P_{\text{beam}}(t)$ curves by a factor of 3, f would need to vary by a factor of 10 in a nonmonotonic way, as in the case of loop length, etc.

6.4. Noncollisional Beam Energy Losses

In beams of high current density, energy losses to driving the neutralizing return current can be more important than collisional losses, especially if wave turbulence enhances resistivity (Emslie 1980; Brown & Hayward 1982; Zharkova et al. 1995). For a given F_{HXR} , this requires a larger beam flux and higher plasma heating rate P_{beam} . The factor is time-dependent and higher for filamented beams.

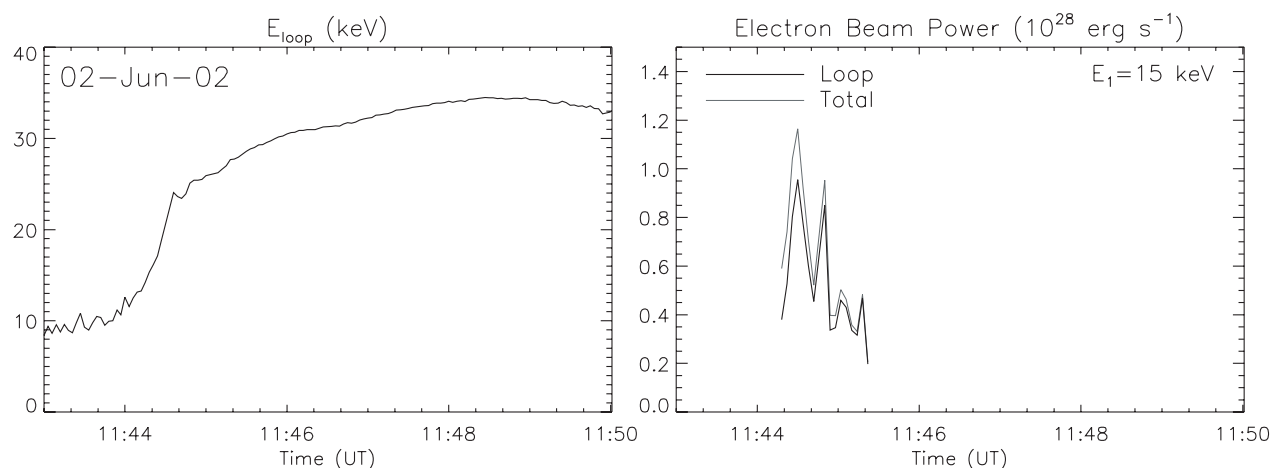


FIG. 16.—Same as Fig. 3, but for the 2002 June 2 flare.

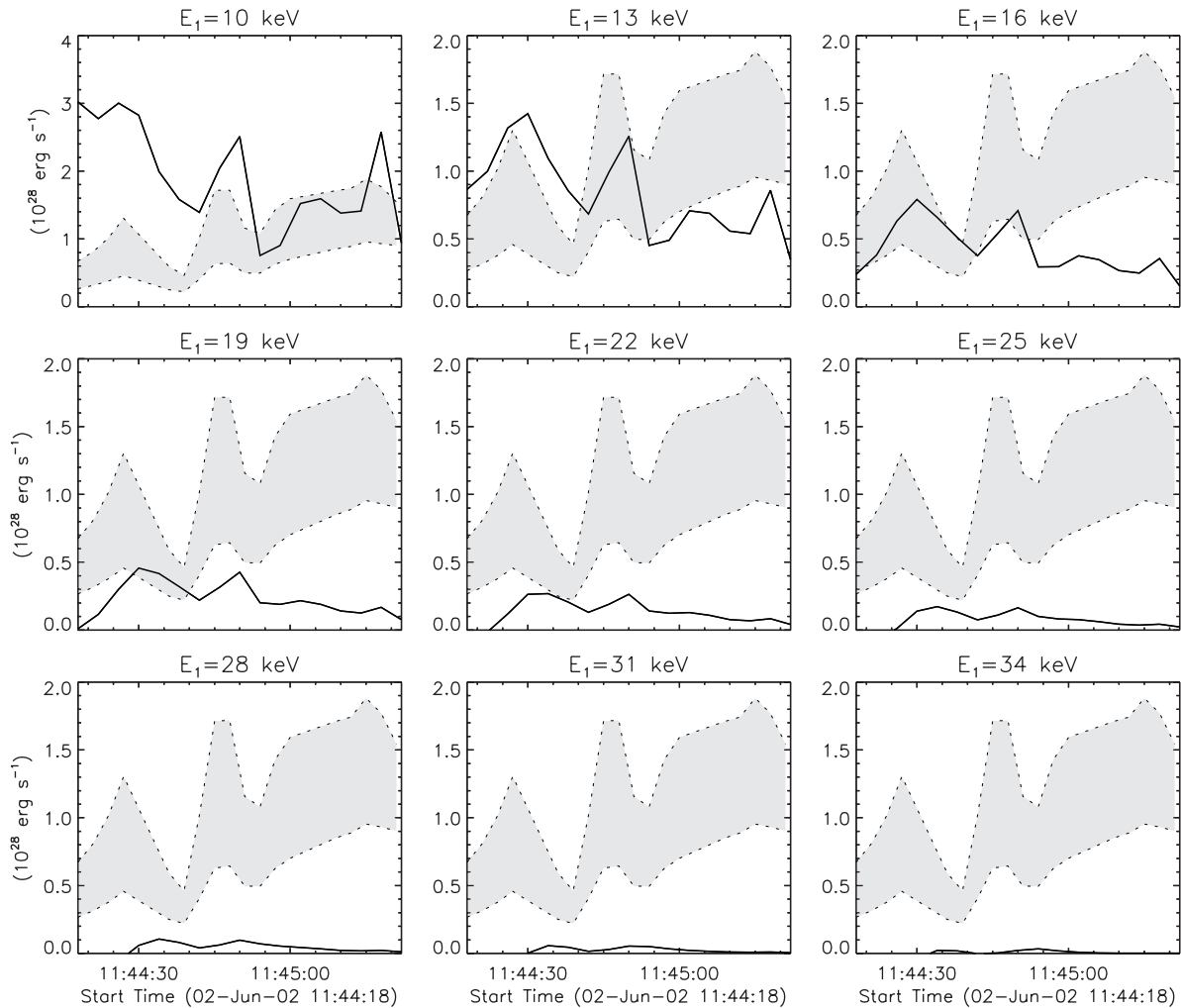


FIG. 17.—Same as Fig. 4, but for the 2002 June 2 flare.

6.5. Additional (Nonbeam) Heating Processes

In none of the four events was it possible to obtain a detailed match between $P_{\text{in}}(t)$ and $P_{\text{beam}}(t)$ for any constant low cutoff energy E_1 . In particular, in the early phase of the flare, $P_{\text{in}}(t)$ is considerably higher than $P_{\text{beam}}(t)$ for the E_1 values derived from the balance of the total SXR plasma and beam energy content (see the 2002 February 20, April 14, and April 15 events). This might be an indication of a “preheating” of the flare atmosphere that is not caused by electron beams but by, for example, direct heating during magnetic reconnection. In the *RHESSI* light curves of these three flares (but not in the 2002 June 2 event), an increase at low (6–12 keV) energies before the impulsive HXR onset at 25–100 keV can be seen. A temporal change in the value of ϕ due to noncollisional (turbulent wave) losses might affect the theoretical power profile shape.

There might even be a direct heating component during the whole flare. For example, Figure 9 shows a very good correlation between the *RHESSI* 25–100 keV flux and the *GOES* time derivative indicative of beam heating, but it also reveals a more gradually varying component in the *GOES* derivative that is similar to the *RHESSI* soft 6–12 keV flux. This gradually varying component could be an indicator of a direct heating process in addition to electron beam heating masking a clear empirical Neupert effect (ENE). Such a second heating agent is expected to cause an even stronger deviation from the

TNE, since for the calculation of $P_{\text{in}}(t)$ it is assumed that the enhanced SXR flare emission is solely due to beam heating (neglecting any possible additional heating process). In this case, the TNE correlations should indeed be worse than the ENE correlations.

The negative result for constant E_1 may at first sight seem somewhat in contrast with the positive outcome from hydrodynamic simulations of the NE for the nonthermal beam model (Li et al. 1993); however, this is not correct, as noted in § 1. What Li et al. (1993) did was show that if an electron beam of constant E_1 heats the coronal loop, then a hydrodynamic simulation leads to an “empirical” NE. But this does *not* mean that if there is an observational NE it requires that the loop be heated by a beam of constant E_1 . Instead, the loop could be directly heated by another mechanism, such as magnetic reconnection with a roughly time-synchronous beam contributing significantly lower (or even no) heating power.

6.6. Time Variation of E_1

If we allow the low cutoff energy E_1 to change during a flare and see how it has to vary in order that $P_{\text{in}}(t)$ and $P_{\text{beam}}(t)$ exactly match at each time step, then we find that only small changes in E_1 are necessary [see the derived $E_1(t)$ for each of the flares in Fig. 18]. This holds in particular for the two April events with their extremely steep spectra. Thus, the low cutoff energy is

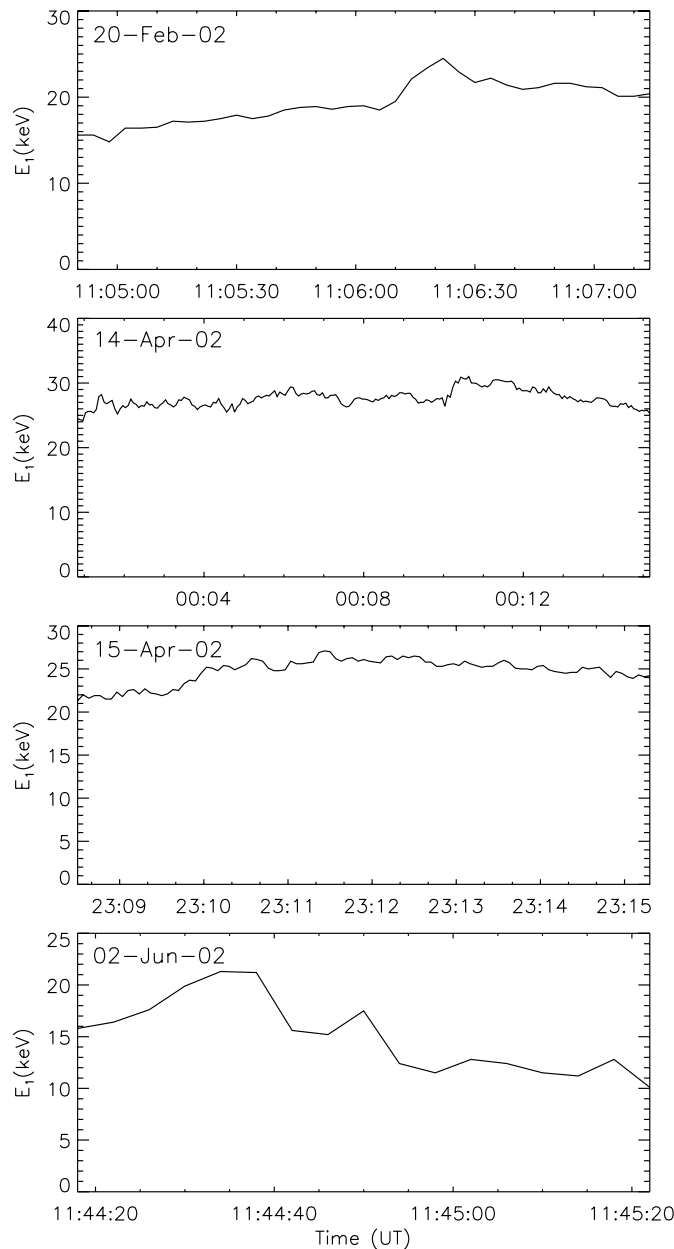


FIG. 18.—For all four events, evolution of the low cutoff energy E_1 derived from the demand (perfect TNE correlation) that at each instant of time $P_{in}(t) = P_{beam}(t)$.

confined to a quite narrow range when we demand a perfect TNE correlation.

L. Sui et al. (2005, in preparation) performed a detailed multiwavelength analysis of the 2002 April 15 event and used a different approach to determine the low cutoff energy based on comparison of the thermal component of the HXR spectra before and after the impulsive increase. Before the impulsive rise of the HXRs, the *RHESSI* spectra were fitted solely with an isothermal bremsstrahlung function. After the impulsive rise, because of the steep nonthermal component, a low cutoff energy of about 30 keV was required in order to get a consistent evolution of the thermal plasma parameters with time.

From the TNE analysis of the 2002 April 15 flare we found a mean $E_1 \approx 25$ keV. In the fit shown in Figure 13 (*RHESSI* spectrum obtained during the maximum of the 25–50 keV emission of the 2002 April 15 flare), E_1 was as a free parameter result-

ing in $E_1 = 17$ keV and $\chi^2 = 1.8$. Repeating the fit but imposing $E_1 = 25$ keV gives a higher $\chi^2 = 3.3$, which might still be consistent with the data (especially if the plasma were non-isothermal). In summary, in all four flares the E_1 derived from the TNE analysis is not inconsistent with the HXR spectra, although it is certainly not the best fit.

6.7. Flaws in the Energy Budget Model

We recognize that, while we have used real flare data, we followed a very simplified model of energy budgets. However, our approximate description of heating and cooling terms and our inclusion of varying EM as well as T in the energy content estimates should be of roughly the right order and should certainly shift the shape of the X-ray flux light curves in the right sense to give an improved correlation of the power curves over the raw data. Uncertainties in the thermal plasma parameters due to calibration and nonisothermality affect the value of this shift but not its direction.

Li et al. (1993) did hydrodynamic simulations using a simple parametric model (producing HXR spikes) for the electron beam input time profile $P_{beam}(t)$ and, from the resulting model hot plasma, predicted theoretical $F_{SXR}(t)$ that broadly resemble those typically observed and show an NE. An interesting next step in theoretical work would be to use a hydrodynamic code applied to specific event data.

6.8. Time-Dependent Fine Structure within the Loop

One fundamental assumption we have made is that the variations within the loop are monolithic in the sense that, even with a filling factor, only one $P_{beam}(t)$ and one $P_{in}(t)$ are relevant at each time. If, below the resolution, the loop comprised a large number of (e.g., fibril) structures, each heated by a distinct $\Delta P_{beam}(t)$ with different time variations, then it would be necessary to revisit the whole energy budget calculation, summing up the contributions of each element. (This would, of course, introduce a rather huge degree of freedom in terms of how the unresolved partitioning into fine structures was chosen and make model testing very difficult. However, see the multiloop modeling approaches by Hori et al. [1997, 1998] and Reeves & Warren [2002].)

One such scenario is that in which the fibril substructures “fire” sequentially, progressing through the overall volume as reconnection proceeds. This is akin to a small-scale unresolved version of the larger scale arcade structures seen particularly in postflare loops by *TRACE* (e.g., Schrijver et al. 1999; Warren 2000). In such a scenario, one would expect that the TNE in each successive fibril would lead to an initial rise to some T -value with a small EM, and thereafter to a fairly steady T (being about the same for each fibril episode) but with a continued rise in EM as more and more fibrils are heated. Indeed, observations indicate such behavior [see, e.g., the $T(t)$ and EM(t) curves for the event of April 14 shown in Fig. 7] and lend some support to this idea. On the other hand, there is a serious theoretical problem with the successive reconnecting fibril scenario. Reasonable though it is in terms of reconnection, the scenario only changes the results of our treatment radically if there are many fibrils, each of an area much smaller than that of our loops. However, fragmenting the plasma in this way does not reduce the instantaneous beam power and total particle injection rate required by the HXR flux. Consequently, to have N fibrils sequentially activated would require a beam with particle and current density higher by a factor of N compared to those in a monolithic loop model. Not only would this move the HXR-emitting beam far into the regime

of beam-plasma instabilities, but it would also result in a loop volumetric heating rate N times larger with likely huge plasma temperatures. In addition, noncollisional energy losses demand an even higher beam power for a specific observed F_{HXR} value, as already noted.

Some authors (Hori et al. 1997, 1998; Reeves & Warren 2002) have modeled multiple energy injections into multiple loop structures and compared the results with SXR observations. While this is certainly an interesting direction for future work, up to now multiple energy injections by beams have not been considered in these multiloop models nor have they been linked to specific HXR observations. At present, it remains unclear whether the small instantaneous activation areas can be reconciled with the beam propagation and plasma heating properties implied by the data. Even apart from beam/return-current stability considerations, too small an instantaneous area A cannot be compatible with the high instantaneous electron injection rate

F (s^{-1}) required for HXR events. Even if every plasma electron were accelerated to speed v ($\approx 10^{10} \text{ cm s}^{-1}$), we are restricted to $F < Anv$ so that, with $F > 10^{36}$ in a large event, $A_{16}n_{10} > 1$. (This certainly rules out identifying A with the area across a single reconnection sheet.) It is to be hoped that progress in physical modeling of the ENE, building from our crude first attempt, will shed important light on these fundamental questions.

A. M. V. thanks Ken Phillips, Gordon Holman, Peter Gallagher, and Dominic Zarro for all their help and many interesting discussions. Financial support by the Austrian Science Fund (FWF grant P15344) is gratefully acknowledged (A. M. V.). J. C. B. gratefully acknowledges support by a UK PPARC grant and by the University of Alabama in Huntsville.

REFERENCES

- Antiochos, S. K., & Sturrock, P. A. 1978, *ApJ*, 220, 1137
 Aschwanden, M. J., & Alexander, D. 2001, *Sol. Phys.*, 204, 91
 Aschwanden, M. J., Brown, J. C., & Kontar, E. P. 2002, *Sol. Phys.*, 210, 383
 Benka, S. G., & Holman, G. D. 1994, *ApJ*, 435, 469
 Berger, T. E., De Pontieu, B., Fletcher, L., Schrijver, C. J., Tarbell, T. D., & Title, A. M. 1999, *Sol. Phys.*, 190, 409
 Brown, J. C. 1971, *Sol. Phys.*, 18, 489
 ———. 1972, *Sol. Phys.*, 26, 441
 ———. 1973, *Sol. Phys.*, 31, 143
 ———. 1974, in *IAU Symp. 57, Coronal Disturbances*, ed. G. A. Newkirk (Dordrecht: Reidel), 395
 Brown, J. C., & Hayward, J. 1982, *Sol. Phys.*, 80, 129
 Cox, D. P., & Tucker, W. H. 1969, *ApJ*, 157, 1157
 Dennis, B. R., & Zarro, D. M. 1993, *Sol. Phys.*, 146, 177
 Elwert, G. 1939, *Ann. Phys.*, 34, 178
 Emslie, A. G. 1978, *ApJ*, 224, 241
 ———. 1980, *ApJ*, 235, 1055
 Emslie, A. G., Kontar, E. P., Krucker, S., & Lin, R. P. 2003, *ApJ*, 595, L107
 Feldman, U. 1990, *ApJ*, 364, 322
 Fisher, G. H., & Hawley, S. L. 1990, *ApJ*, 357, 243
 Garcia, H. 1994, *Sol. Phys.*, 154, 275
 Haug, E. 1997, *A&A*, 326, 417
 Hawley, S. L., & Fisher, G. H. 1994, *ApJ*, 426, 387
 Holman, G. D. 2003, *ApJ*, 586, 606
 Holman, G. D., & Benka, S. G. 1992, *ApJ*, 400, L79
 Holman, G. D., Sui, L., Schwartz, R. A., & Emslie, A. G. 2003, *ApJ*, 595, L97
 Hori, K., Yokoyama, T., Kosugi, T., & Shibata, K. 1997, *ApJ*, 489, 426
 ———. 1998, *ApJ*, 500, 492
 Hoyng, P., Brown, J. C., & van Beek, H. F. 1976, *Sol. Phys.*, 48, 197
 Hudson, H. S. 1972, *Sol. Phys.*, 24, 414
 ———. 1991, *BAAS*, 23, 1064
 Hudson, H. S., Strong, K. T., Dennis, B. R., Zarro, D., Inda, M., Kosugi, T., & Sakao, T. 1994, *ApJ*, 422, L25
 Hurford, G. J., et al. 2002, *Sol. Phys.*, 210, 61
 Kosugi, T., Sakao, T., Masuda, S., Hara, H., Shimizu, T., & Hudson, H. S. 1994, in *Proc. Kofu Symp.*, ed. S. Enome & T. Hirayama (Nagano: Nobeyama Radio Obs.), 127
 Krucker, S., & Lin, R. P. 2002, *Sol. Phys.*, 210, 229
 Lee, T. T., Petrosian, V., & McTiernan, J. M. 1995, *ApJ*, 448, 915
 Li, P., Emslie, A. G., & Mariska, J. T. 1993, *ApJ*, 417, 313
 Lin, R. P., & Hudson, H. S. 1976, *Sol. Phys.*, 50, 153
 Lin, R. P., et al. 2002, *Sol. Phys.*, 210, 3
 McTiernan, J. M., Fisher, G. H., & Li, P. 1999, *ApJ*, 514, 472
 Mewe, R., Gronenschild, E. H. B. M., & van den Oord, G. H. J. 1985, *A&AS*, 62, 197
 Neupert, W. M. 1968, *ApJ*, 153, L59
 Phillips, K. J. H. 2004, *ApJ*, 605, 921
 Piana, M., Brown, J. C., & Thompson, A. M. 1995, *Sol. Phys.*, 156, 315
 Reeves, K. K., & Warren, H. 2002, *ApJ*, 578, 590
 Schmahl, E., & Hurford, G. 2002, *Sol. Phys.*, 210, 273
 Schrijver, K., et al. 1999, *Sol. Phys.*, 187, 261
 Schwartz, R. A., Csillaghy, A., Tolbert, A. K., Hurford, G. J., McTiernan, J., & Zarro, D. 2002, *Sol. Phys.*, 210, 165
 Smith, D. M., et al. 2002, *Sol. Phys.*, 210, 33
 Sui, L., & Holman, G. D. 2003, *ApJ*, 596, L251
 Sui, L., Holman, G. D., & Dennis, B. R. 2004, *ApJ*, 612, 546
 Sui, L., Holman, G. D., Dennis, B. R., Krucker, S., Schwartz, R., & Tolbert, K. 2002, *Sol. Phys.*, 210, 245
 Sweet, P. A. 1969, *ARA&A*, 7, 149
 Thomas, R. J., Starr, R., & Crannell, C. J. 1985, *Sol. Phys.*, 95, 323
 Veronig, A. M., & Brown, J. C. 2004, *ApJ*, 603, L117
 Veronig, A., Temmer, M., Hanslmeier, A., Otruba, W., & Messerotti, M. 2002a, *A&A*, 382, 1070
 Veronig, A., Vršnak, B., Dennis, B. R., Temmer, M., Hanslmeier, A., & Magdalenic, J. 2002b, *A&A*, 392, 699
 Veronig, A., Vršnak, B., Temmer, M., & Hanslmeier, A. 2002c, *Sol. Phys.*, 208, 297
 Vilmer, N., Krucker, S., Lin, R. P., & the *RHESSI* Team. 2002, *Sol. Phys.*, 210, 261
 Warren, H. P. 2000, *ApJ*, 536, L105
 Webb, D. F. 1985, *Sol. Phys.*, 97, 321
 White, S. M., Thomas, R. J., & Schwartz, R. A. 2004, *Sol. Phys.*, submitted
 Young, P. R., Del Zanna, G., Landi, E., Dere, K. P., Mason, H. E., & Landini, M. 2003, *ApJS*, 144, 135
 Zharkova, V. V., Brown, J. C., & Syniavskii, D. V. 1995, *A&A*, 304, 284